

Studies of Kinetic Models for Oxidation Reactions over Metals (Exemplified by CO Oxidation)

1. Mechanisms and models

The fundamentals of the kinetics for heterogeneous catalysis had been based, in 1910–1920, on the data obtained from studies of the oxidation of simple molecules over metals, primarily of CO and H₂ over Pt (see Langmuir's classical studies [1, 2]).

During the years which followed, oxidation reactions over metals became the objects for systematic studies. The most studied was CO oxidation over Pt metals, i.e. a reaction that is both relatively simple and also important from the ecological viewpoint (after burning of industrial and exhaust gases). In the last decade, CO oxidation has become a model for testing the newest physical methods for studying the structure and composition of catalysts, i.e. low-energy electron diffraction (LEED), Auger electron spectroscopy (AES), X-ray photoelectron spectroscopy (XPS), molecular beam techniques etc. We hope that it will be in this CO oxidation that the elimination of the so-called "pressure-gap" problem will be solved in the near future. The aim is to construct a general model that will provide a description for both high-vacuum experimental data and those of industrial catalysis (10^{-1} – 10^3 Torr).

CO oxidation over Pt metals (Pt, Pd, Ir, Ru, Rh) is a complex reaction. For its description, various steps are used from the mechanisms



where ZO, ZCO, and Z are the adsorbed oxygen, CO, and unoccupied surface sites, respectively, and $k_{\pm i}$ are the rate constants for elementary reactions. Mechanism (1) includes two routes: "impact" [steps (1) and (4)] and "adsorption" [steps (1)–(3)]. The "impact" mechanism is often called the Eley–Rideal (E–R) mechanism and the "adsorption" mechanism is referred to as the

Langmuir-Hinshelwood mechanism. Strictly speaking, however, this is incorrect since both of these mechanisms date back to Langmuir*.

The solution of the dilemma as to whether it is an "impact" or an "adsorption" mechanism was the framework within which many catalytic reactions were studied. Evolution in the interpretation of CO oxidation over noble metals (in high-vacuum experiments) can be characterized in a rather simplified form by the three periods: I, from Langmuir studies until the 1970s the traditional impact (E-R) mechanism; II, during the first half of the 1970s, a combination of the impact (E-R) and adsorption mechanisms; and III, the present time starting in the second part of the 1970s. In our opinion, this period is characterized by two major viewpoints: (1) CO oxidation follows the adsorption mechanism (this viewpoint was reported in the pioneering studies of Palmer and Smith [4] and Malakhov et al. [5]) whose kinetic characteristics (reaction rate constants) depend significantly on the surface composition, (2) alongside the adsorption mechanism, there is a contribution from the interaction of adsorbed oxygen with CO in the pre-adsorption state ("precursor state"). This mechanism can be treated as either a modified impact or any other version of the adsorption mechanism. Langmuir (ref. 1, p. 61) wrote: "The experimental evidence with carbon monoxide and oxygen on platinum proves that nearly, but not quite all of the reaction between these gases occurs during collision of carbon monoxide molecules with the oxygen covered surface". It is likely that the author prefers the impact mechanism. However, later on he says: "In a reaction of this kind which occurs as the result of collisions, we may expect that in some cases the exposure of the 'flanks' of an adsorbed film to attack by colliding molecules may render them much more susceptible to chemical action. For example, it is conceivable - although in this particular case there is no experimental evidence for it - that, if the whole surface of platinum were covered by oxygen atoms, incident carbon monoxide molecules should be unable to react, while if only a certain limited portion of the surface were covered with oxygen, the monoxide molecules striking the oxygen atoms close to the place where they are attached to the platinum, might be able to react. In this case the oxygen film would be removed progressively from its bounding edge inward." Hence, according to Langmuir, the collision mechanism can be complex. It is far from being a simple "frontal" interaction between adsorbed oxygen and gaseous CO.

* This was noted by Temkin at the Soviet-Japanese Seminar on Catalysis (Novosibirsk, 1971) and also by Krylov [3]. Let us cite a very typical suggestion made by Langmuir ref. 1, p. 616: "The reaction which takes place at the surface of a catalyst may occur by interaction between molecules or atoms adsorbed in adjacent spaces on the surface, or it may occur between an adsorbed film and the atoms of the underlying solid, or again, it may take place directly as a result of a collision between a gas molecule and an adsorbed molecule or atom on the surface. This third kind of action is perhaps indistinguishable from one in which the incident gas molecules condense on top of those already on the surface, and then react before they have a chance to evaporate."

The evolution of the concepts of the CO oxidation mechanism is shown in Table 1. Surveys of modern viewpoints on the separate steps of this complex reaction (1) can be found in the literature [6–35].

We shall give brief characteristics of the various steps, proceeding from the high-vacuum experimental data.

Adsorption-desorption of oxygen. As a rule, oxygen adsorption over Pt metals is dissociative with practically zero activation energy [12–14, 41–50, 64–76].

Sticking coefficients are given in Table 2. At $T > 300$ K and $P > 10^{-6}$ Torr, molecular adsorption can also take place [12, 16, 38, 39, 76]. According

TABLE 1

Evolution in the concepts of the mechanism of CO oxidation in ultrahigh vacuum (10^{-9} to 10^{-6} Torr)

Mechanism	Catalyst	Ref.
$\text{CO}_{\text{gas}} + \text{O}_{\text{ads}}$	Pt	2
$\text{CO}_{\text{gas}} + \text{O}_{\text{ads}}$	Pd(110)	36
$\text{CO}_{\text{gas}} + \text{O}_{2,\text{ads}}$	Pt	37, 38
$\text{CO}_{\text{gas}} + \text{O}_{\text{ads}}$	Pd	39
$\text{CO}_{\text{gas}} + \text{O}_{2,\text{ads}}$	Pt	40
$\text{CO}_{\text{gas}} + \text{O}_{\text{ads}}$	Ir(110)	41
$\text{CO}_{\text{gas}} + \text{O}_{\text{ads}}$	Pt	42
$\text{CO}_{\text{ads}} + \text{O}_{\text{ads}}$	Pt(110)	43
	Pd(110)	44
$\text{CO}_{\text{gas}} + \text{O}_{\text{ads}}$	Pt	45
	Pt	46
	Ru(001)	47
	Pd	9
	Pt	48
	Ir(111)	50
	Pt	51
$\text{CO}_{\text{ads}} + \text{O}_{\text{ads}}$	Pt(110)	4
	Pt	5
	Pd(111)	52
	Pt	53
	Ir	54
	Ir(110)	55
	Rh	56
	Ir(111)	57
$\text{CO}_{\text{ads}} + \text{O}_{\text{ads}}$	Ir(111)	58, 59
$\text{CO}_{\text{pre}} + \text{O}_{\text{ads}}$	Pd	60
	Pt	61, 62
	Rh	8

TABLE 2

Oxygen chemisorption over Pt metals

Catalyst, surface orien- tation	Sticking coefficient S_{O_2}	E_{-1} (kcal mol ⁻¹)	Ref.
Pt stepped	0.16	50 ± 3	77
Pt polycryst.	0.45	50 ± 3	77
Pt(111)	0.02	50 ± 3	77
Pt(111)	0.08-0.1		69
Pt(111)	10 ⁻²	57-45	13
Pt(111)	10 ⁻³		67
Pt(111)	0.4	45 ± 4	16
Pt(100)	4 × 10 ⁻⁴	45	66
Pt(110)	0.4		74
Pt(110)	0.13	30	63
Pt polycryst.	0.14	58	64, 65
Pt polycryst.	0.25	44 ± 2	42
Pt polycryst.	0.05	~ 40	11
Pt polycryst.	0.2(monomolec.)	17	37, 38
Pt polycryst.	10 ⁻⁷ -10 ⁻⁸		12
Pt polycryst.	0.36		61
Pd(111)	0.3	55	44
Pd(110)		80-48	36, 44
Pd polycryst.	0.8-1		60
Pd polycryst.	0.35	51 ± 2	73
Ru(001)	0.75	80	47
Ru(101)	0.004	72	71
Rh polycryst.	0.1		8
Ir(100)	0.26	80 ± 6	72
Ir(110)		53 ± 4	41
Ir(111)	0.05	70	50
Ir(111)	0.045	65-10 θ_0	59, 78
Ir(110)	0.26	56-3 θ_0	78
Ir(110) pure oxidized	0.28 0.4	70-45 (falls with increasing θ_0)	76

to Tretiakov et al. [37-39], it is the molecular form of oxygen that is reactive at high pressures.

On metal surfaces, well-ordered structures are often formed [7, 79-82]. At sufficiently high temperatures (> 300 K) and pressures (> 10⁻⁶ Torr), oxygen diffuses into the catalyst bulk [8, 61, 73-76, 83-91]: in Pd, as many as 300 monolayers are dissolved [83] whereas in Ir and Pt the number of dissolved monolayers is slightly lower [78, 85-87]. The oxygen dissolved in the subsurface layer changes the reaction rate constants considerably (see Table 3 [86]). Finally, under certain conditions, oxygen adsorption can lead to surface reconstruction [7, 92]. Various types of oxygen adsorption over Pt metals have been studied in detail by Savchenko [7].

TABLE 3

Properties of "chemisorbed" and "subsurface" oxygen on Pt(111) [86]

Properties	"Chemisorbed" oxygen	"Oxide"
Generation by O ₂ exposure at	$T < 800$ K	$T > 800$ K
Desorption	Slowly at $T > 550$ K, completely at $T \sim 1000$ K	Slow decomposition at $T \approx 1200$ K
Reaction with H ₂ and CO	Removed even at room temperature, "reactive"	Not removed, even at 1000 K, "non-reactive"
Binding energies of H ₂ and CO	As on clean Pt (because oxygen is removed in the presence of H ₂ and CO)	New states with higher binding energies than on clean Pt
Catalytic activity	As on clean Pt (because oxygen is removed in the presence of H ₂ and CO)	Larger activity and changed selectivity compared with clean Pt
Main IR bands of adsorbed CO	2060–80 cm ⁻¹ as on clean Pt Type I	New band at 2120 cm ⁻¹ Type II
Position of oxygen	496 and 517 eV	491 and 511 eV
Auger peak (chemical shift)	($\Delta \approx 6$ eV)	($\Delta \approx 6$ eV)
Work function change with respect to clean Pt	+ 0.5 eV	- 1 eV

It must be noted that the sticking coefficient of oxygen depends on the surface composition: the adsorbed CO and O₂ inhibit dissociative adsorption [60, 66, 76]. Oxygen desorption is also a complex process. Thermodesorption spectra exhibit up to five oxygen states [68]. At low surface coverage, the kinetic desorption curve is of the second order, whereas at high surface coverage it is of the first order. The activation energy depends essentially on the surface composition, primarily on the concentration of surface oxygen.

The description of kinetic dependences is, however, facilitated considerably by the fact that the desorption activation energy is sufficiently high (> 50 kcal mol⁻¹) for desorption to be neglected at $T < 700$ K.

Adsorption-desorption of CO. CO adsorption is monomolecular. On all the Pt metals except Ir it proceeds through the pre-adsorbed ("precursor") state [17, 93]. The activation energy is practically zero and the initial sticking coefficient is high (0.5–1.0). Oxygen does not inhibit CO adsorption [55, 94]. The sticking coefficient is weakly dependent on the surface concentration of CO. During the adsorption on Ru and Ir, surface carbides can form.

Desorption kinetic curves are of the first order. The activation energy is in the 25–40 kcal mol⁻¹ range and depends on the surface concentrations of CO (primarily) and O₂. Some literature data on the parameters for CO chemisorption over Pt metals are listed in Table 4. Comprehensive surveys of CO chemisorption were made by Ford [24] (up to 1970), Sklyarov [25] (thermodesorption and IR spectroscopic data) and Bredshaw [21]. Mention should also be made of the studies performed at the Institute of Catalysis, Siberian Branch of the U.S.S.R. Academy of Sciences [5, 58, 59, 67, 78, 87, 92, 99–106].

TABLE 4

CO chemisorption over Pt metals

Catalyst, surface orientation	Sticking coefficient, S_{CO}	k_{-2}^0 (s ⁻¹)	E_{-2} (kcal mol ⁻¹)	Ref.
Pt(111)	0.5	10 ¹³	28	77
Pt stepped	0.7	10 ¹³		77
Pt polycryst.	1.0	10 ¹³	35	77
Pt(111)		10 ¹³	33–40	95
Pt(111)	0.5	10 ¹³	32	11
Pt(111)	0.45	10 ¹³	31	67
Pt polycryst.	0.3		28.5	5
Pt polycryst.		5 × 10 ¹¹	22	23
		5 × 10 ¹¹	25.7	
		1 × 10 ¹²	28.5	
		1 × 10 ¹²	31.7	
		1 × 10 ¹²	33.5	
Pt polycryst.	0.5	10 ¹³	34	42
Pt(110)		10 ¹³	32	66
Pt(111)	0.34		29.6	22
Pt(110)			26	84
Pd(111)	1.0	10 ¹³	36.5	18, 44
Pd(110)	1.0		40	18
Pd(100)	1.0		36.5	96
Pd(111)	0.96	10 ^{14.4±0.8}	32 ± 2	98
Pd polycryst.		10 ^{7–10¹²} (Falls with increasing θ_{CO})	15–30 (Falls with increasing θ_{CO})	73
Ir(111)	0.9	10 ¹³	32	93
Ir(110)	0.9	10 ¹³	37	14
Ir(110)	1.0	10 ¹³	35	78
Ir(111)	0.75	10 ¹³	33	78
Ir(110)		10 ¹⁰	35–16 θ_{CO}	94
Ru(001)	0.57	10 ¹³	29	47
Ru(101)	0.85	10 ¹³	30	71
Ru(1010)		10 ¹³	30.1	97
			24.4	
Rh polycryst.	1.0	3.5 × 10 ¹³	31.5	8

The CO₂ formation step. We have already spoken about the adsorption or impact mechanism dilemma we are facing in the interpretation of data concerning the CO oxidation over Group VIII metals.

Let us discuss it in more detail. The concept of the impact mechanism (E-R) was most firmly defended by Tretiakov et al. who studied this reaction at relatively high pressures (10^{-5} to 10^{-1} Torr) [37-39]. Among the reactive forms they considered were molecular oxygen for the oxidation over Pt [37, 38] and atomic oxygen in the oxidation over Pd [39]. The adsorbed CO does not participate in the formation of CO₂. A similar viewpoint was reported by Ertl and Rau in their earlier study [36].

Early in the 1970s, some proof was obtained of the shortcomings of the impact mechanism concept and the necessity of its modification. On the one hand, it was shown [43] that, if oxygen is pre-adsorbed on the Pt surface (at $T > 263$ K), its reaction with CO in the gas phase was always immediate. The formation rate of CO₂ was independent of temperature. This fact agrees with the impact mechanism concept. But in the same study during the interaction of adsorbed CO with gaseous oxygen ($T = 373$ - 493 K) the authors [43] observed induction periods. The formation of CO₂ as a result of the interaction between chemisorbed CO and oxygen was also observed [44]. It was these facts that made it necessary to apply the concept of the adsorption mechanism. The first attempts were rather timid: despite the obvious arguments in favour of the Langmuir-Hinshelwood (L-H) mechanism, the domination of the Eley-Rideal (E-R) mechanism was still asserted.

The two-route mechanism (1) was qualitatively substantiated by Winterbottom [45]. A system of steps corresponding to this mechanism was first given by Kuchaev and Nikitushina [46] who also studied a steady-state kinetic model. Rate constants for mechanism (1) were reported by Cassuto et al. [48, 49, 65, 107, 108]. All except k_3 were determined using the molecular beam method. The value for k_3 was obtained from the solution of the inverse problem. It is these constants that will be applied by us here.

New experimental data led to more severe revision of the impact mechanism concept. It appeared that the rate of the adsorbed oxygen titration by gaseous CO at high concentrations of surface oxygen (θ_0) is practically independent of θ_0 [58, 60, 62, 108-110], i.e. the relationship $W_{\text{CO}_2} = W_{\text{E-R}} = k_4 P_{\text{CO}} \theta_0$ corresponding to the E-R mechanism is not satisfied. At present the pendulum has swung to the opposite side and most research workers [98] are sure that, over a wide range of the reaction parameters ($T = 450$ - 950 K, $P = 10^{-7}$ to 10^{-5} Torr), only the adsorption mechanism (L-H) is valid. This belief is based on the data obtained in unsteady-state experiments and using modern physical methods, in particular the molecular beam technique [98, 52, 107]*. But a fairly good qualitative description on the basis of the L-H mechanism has been obtained in only a few cases [56, 57] and this description concerns rather limited experimental

* Particularly emphasized must be the study of Malakhov et al. [5] who suggested that CO oxidation follows only the adsorption mechanism.

data. (Only recently, the situation has changed for the better.) For example, Campbell et al. [56] applied the L-H mechanism to describe the titration of adsorbed oxygen by gaseous CO (Rh catalyst). They assumed that: (1) the formation energy of CO₂, $E_3 = E_{L-H}$, depends on the oxygen surface coverage; (2) CO adsorption is inhibited by oxygen at $T > 529$ K; and (3) the parameters of CO₂ formation change sharply when the reaction temperature attains 529 K. At $T \geq 529$ K, $k_3^0 = 2.76 \times 10^{11} \text{ s}^{-1}$, $E_3 = 25 \text{ kcal mol}^{-1}$, and $T < 529$ K, $k_3^0 = 1.14 \times 10^6 \text{ s}^{-1}$ and $E_3 = 14.3 \text{ kcal mol}^{-1}$.

Küppers and Plagge [57] described steady-state kinetic dependences for CO oxidation over Ir(111) at only one composition of the gas mixture $P_{O_2} = P_{CO} = 1 \times 10^{-7}$ Torr. They obtain experimental data for the dependence of the sticking coefficient for O₂ and CO on the surface composition, activation energies of CO adsorption, and also $k_3^0 = 6.1 \times 10^6 \text{ s}^{-1}$ and $E_3 = 10.7 \text{ kcal mol}^{-1}$. But the facts of the high reactivity for the adsorbed oxygen at low (below 80 K) temperatures and constant steady-state rates over a wide temperature range can hardly be interpreted in terms of the "pure" L-H mechanism without introducing some additional complicating assumptions. We can state that the simple equation $W_{CO_2} = W_{L-H} = k_3 \theta_O \theta_{CO}$ (where θ_{CO} is the concentration of the adsorbed CO) corresponding to the L-H mechanism cannot describe experiments over a wide range of their parameters. We must take into account the dependence of the reaction rate constants on the surface composition [111] and the treatment conditions for the catalyst. Apparently, in a certain range of temperatures and surface coverages, the adsorbed oxygen is localized as "islands". The model must account for the surface diffusion of the adsorbed CO towards the boundaries of these islands and it is as these boundaries where the reaction takes place. The reaction rate can be limited by the rate of the surface diffusion [55]. Values of the parameters of the L-H mechanism are uncertain. The literature data fall into two groups (Table 5): (1) $E_3 \leq 8\text{--}12 \text{ kcal mol}^{-1}$ [5, 72, 55, 57, 78, 112], $k_3^0 \cong 10^{-11}$ (ranges within 10^{-9} to $10^{-12} \text{ cm}^2 \text{ molecule}^{-1} \text{ s}^{-1}$) [5, 55, 57, 78, 112]; (2) $E_3 > 20 \text{ kcal mol}^{-1}$ [45, 48, 49, 51, 52], $k_3^0 \cong 10^{-3} \text{ cm}^2 \text{ molecule}^{-1} \text{ s}^{-1}$ [48, 57]. The latter value is closer to that obtained using the transition-state method.

Matsushima et al. [60, 61] interpreted their experimental data with a two-route mechanism. They treated the adsorption mechanism (L-H) as that which (a) involves the participation of strongly bonded molecules of CO and (b) has high activation energies for CO₂ formation.

The impact mechanism (E-R) is that (a) which involves the participation of weakly bonded ("pre-adsorbed") CO, (b) whose reaction rate is first-order with respect to P_{CO} , (c) where the activation energy for the CO₂ formation is extremely low, and (d) where the reaction rate remains practically unchanged over the range from $\theta_o = 1$ to $\theta_o = \theta_o^*$ and falls with further decreases in θ_o .

According to the Campbell and White data [8] for the CO oxidation over Rh

TABLE 5

CO interaction with O₂ over Pt metals

Catalyst	E_3 (kcal mol ⁻¹)	k_3^0 (cm ² molec ⁻¹ s ⁻¹)	E_4 (kcal mol ⁻¹)	Ref.
Pt foil	22	10 ⁻³	0.5	48
Pt foil	29		0	49
Pt polycryst.	23		0	45
Pt(110)	7.8	1.8 × 10 ⁻¹¹	Unmeasured	112
Pt polycryst.	9.6		0	113
Pt recryst.	6-8	10 ⁻⁹	No	5, 102
Pt polycryst.	23	5 × 10 ⁻⁶	0	114, 51
Pd(111), (100)	7		3	36, 44
Pd(111)	25-14		No	52
Ir(111)	10.7	4 × 10 ⁻⁹		57
Ir(110)	12	3 × 10 ⁻⁹ -3 × 10 ⁻¹⁰		55
Ir polycryst.	10	10 ⁹ s ⁻¹		72
	20	10 ⁸ s ⁻¹		72
Ir(110)	10 ± 1.5	10 ⁻¹¹ -10 ⁻¹²	0	78
Ir(111)	10.5 ± 1.5	10 ⁻¹⁰ -10 ⁻¹¹	0	78
Ru(001)	15			47
Ru(101)	9			71
Rh polycryst.	25	5.5 × 10 ⁻⁴	No	56
		($T > 530$ K)		
	14.3-4.4θ _o	2.3 × 10 ⁻¹¹		
		($T < 530$ K)		

$$W_{E-R} = k_{E-R} P_{CO} \left(\frac{\theta_o}{\theta_o^*} \right)^\kappa$$

where

$$\kappa = \begin{cases} 1, & \theta_o < \theta_o^* \\ 0, & \theta_o \geq \theta_o^* \end{cases}$$

It often happens that $\theta_o < \theta_o^*$, hence the reaction rate takes its ordinary form

$$W_{E-R} = \left(\frac{k_{E-R}}{\theta_o^*} \right) P_{CO} \theta_o$$

The impact mechanism involving the participation of weakly bonded CO can also be treated as a second type of the adsorption mechanism [60, 61]. The approach used by Matsushima et al. [60, 61] has proved to be effective for the interpretation of experimental data. We also think it would be expedient to select a model corresponding to the two-route mechanism. It is this model that will be used to describe the CO oxidation over Pt metals.

As far as the kinetic data obtained under conditions of "real" catalysis (catalysts are polycrystalline metals or supported samples and pressures

high) are concerned, so far we must speak about their informative interpretation with great care. In this case the situation is much worse than when interpreting the high-vacuum experimental data. The reason is obvious: the literature lacks direct data about the surface composition of the catalysts. It is for this reason that the available literature concepts are rather conflicting.

Kinetic equations are often represented as semi-empirical relationships

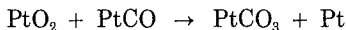
$$W_{\text{CO}_2} = kP_{\text{O}_2}^m P_{\text{CO}}^n$$

where, for example, $m = 1$, $n = -1$ [115, 116] or [117]

$$W_{\text{CO}_2} = \frac{kP_{\text{O}_2}P_{\text{CO}}}{(1 + kP_{\text{CO}})^2}$$

Nevertheless, at present a distinct tendency is observed not to restrict oneself to the semi-empirical equations, but to apply kinetic models corresponding to the physico-chemical substantiated mechanisms. As a rule, modifications of the well-known adsorption (L-H) and impact (E-R) mechanisms are used. As usual, the complex mechanism always has a constituent accounting for the adsorption mechanism.

The applied L-H mechanisms are different. They are associated with different concepts about the character of reactive forms. In accordance with Schwab and Gossner [115], the reaction follows the L-H mechanism with the participation of molecular oxygen. According to Heyne and Tompkins [113], the mechanism includes the steps



The Baddour et al. mechanism [116] consists of the steps

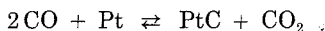


It is this mechanism that corresponds to the expression $W_{\text{CO}_2} = kP_{\text{O}_2}^m P_{\text{CO}}^n$, where $m = 1$ and $n = -1$ (the limiting step is assumed to be the O_2 adsorption) or $m = 1$ and $n = -2$ [the limiting step is suggested to be either CO adsorption or reaction (4)].

Stephens [118] obtained experimental evidence for the adsorption mechanism: during the interaction of CO adsorbed on the catalyst surface with the gas-phase oxygen, he observed long induction periods (~ 1000 min).

In accordance with Hori and Schmidt [119], CO oxidation follows the

adsorption mechanism over a wide range of parameters. They examined steady-state and unsteady-state reaction characteristics and found some interesting kinetic peculiarities, in particular two maximum peaks for the steady-state rate and three different relaxation times. They ascribed these peculiarities to the formation and decomposition of mono- and multi-layer complexes on the catalyst surface. The most probable is the formation of PtC in the disproportionation reaction



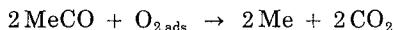
Voltz et al. [117] postulated an adsorption mechanism involving the participation of atomic oxygen. On its basis they obtain the equation

$$W_{\text{CO}_2} = \frac{kP_{\text{O}_2}P_{\text{CO}}}{(1 + kP_{\text{CO}})^2}$$

Eigenberger [120, 121] and Herz and Marin [122] also applied the adsorption mechanism.

At the present time, the mechanisms in which the L-H mechanism is completed by the E-R mechanism are widespread. This two-route mechanism was first suggested by Heyne and Tompkins [113]. The same mechanism was offered by Stephens [118], Hori and Schmidt [119], and McCarthy et al. [123]. McCarthy et al. applied the two-route mechanism to interpret the extreme character of the kinetic dependences and the rate self-oscillations. Miniscloux et al. used the kinetic model corresponding to the two-route mechanism to calculate the catalytic reoxidation of CO in exhaust gases.

Cant et al. [125] suggested a three-route mechanism in which the reactive forms were adsorbed CO and atomic and molecular (physically adsorbed) oxygen. They suggested the existence of step



Analysis of the literature data implies that, for the present, authors should not use the concepts associated only with E-R mechanism for the description of kinetic dependences for CO oxidation.

In our opinion, the most important problem is to establish whether it is possible to apply the kinetic models and parameters obtained in high-vacuum experiments to real catalytic processes.

Bonzel [126] suggested that, during CO oxidation over Pt(110), when going into the region of "real" catalysis, the mechanism remains unchanged but the efficiency of the reaction with respect to CO, i.e. the number of CO₂ molecules produced per molecule of gaseous CO, falls sharply (by about 7 orders of magnitude). A similar conclusion arrived at by Boudart et al. [127, 128] from the analysis of hydrogen oxidation on the Pt/SiO₂ catalyst at low and high pressures. To describe the data obtained by McCarthy et al. under normal conditions [123], it is necessary [125] to decrease the rate constant for

the impact step $\text{CO} + \text{MeO}$ compared with its value obtained at high resolutions*.

The question then arises as to how to explain this sharp decrease in the parameters. Boudart et al. [127, 128] ascribe it to the significant decrease in the surface coverage by oxygen, but the surface coverage must depend on the parameters of the elementary processes taking place in the system: the primary reason must be simply the value of the parameter. Apparently, the sharp drop in the model parameters must be attributed to the decreased number of active surface sites of the catalyst due to the formation of inactive oxides or PtC complexes [119, 122]. The model must account for the catalyst deactivation [122, 125].

High-vacuum experimental results imply that the parameters of individual steps depend on the surface composition (see, for example, refs. 55–57 and 94). It appears that these dependences should also be taken into consideration at normal pressures. In this way Ali and Hugo [111] and Herz and Marin [122], made an attempt (a successful one, in our opinion) to construct a kinetic model with “reasonable” parameters. The kinetic model [111] described self-oscillations of the reaction rate in terms of the two-route mechanism. All parameters of this model (except the CO adsorption constant) were dependent on the surface composition. The model [122] accounted for the decrease in the bond energy of CO on supported Pt and the deactivation of a large number of active sites due to the formation of inactive surface oxides. The authors [111, 122] used parameter values close to those found in high-vacuum experiments. We must also note the study [129] which utilized the model corresponding to the two-route mechanism for the description of thermokinetic oscillations in the CO oxidation rate. It can be stated that nowadays a tendency is observed to construct general kinetic models capable of overcoming the “pressure gap”. It is quite natural that these models are based on the concepts elaborated in high-vacuum experiments (see refs 130–135 for recent studies). It is evident that these attempts would be successful only when the ever-increasing possibilities of modern physical methods are used. We believe that it is only the beginning of the trend.

2. Modelling of kinetic dependences

Mechanism (1) is accounted for by the kinetic model

* One exception [124] claims that, for the description of the experimental data obtained at high pressures, it is not necessary to change the kinetic model constructed on the basis of the data obtained at 10^{-8} to 10^{-7} Torr. (Only the activation energy for the CO desorption was decreased from 34 to 24.5 kcal mol⁻¹.) This claim does not seem to be confident since the discussed kinetic model was only a unit in the model for the catalytic re-oxidation of CO and hydrocarbons. Experimental and calculated data were only compared on the basis of the observed values, i.e. temperature and the amount of unreacted CO in the output.

$$\begin{aligned}
 P(\theta_o, \theta_{CO}) &= \frac{d\theta_o}{dt} \\
 &= 2k_1 P_{O_2} (1 - \theta_o - \theta_{CO})^2 - 2k_{-1} \theta_o^2 - \\
 &\quad - k_3 \theta_o \theta_{CO} - k_4 P_{CO} \theta_o
 \end{aligned} \tag{2}$$

$$\begin{aligned}
 Q(\theta_o, \theta_{CO}) &= \frac{d\theta_{CO}}{dt} \\
 &= k_2 P_{CO} (1 - \theta_o - \theta_{CO}) - k_{-2} \theta_{CO} - k_3 \theta_o \theta_{CO}
 \end{aligned} \tag{3}$$

where θ_o and θ_{CO} are the dimensionless concentrations of the adsorbed oxygen and carbon monoxide, respectively, P_{O_2} and P_{CO} are the partial pressures of gases (assumed to be constant), and $k_{\pm i}$ are the rate constants dependent on the temperature according to the Arrhenius law.

The model (2)–(3) differs from the above model of the adsorption mechanism (7) in Chap. 5 only by the presence in eqn. (2) of the term $k_4 P_{CO} \theta_o$, which corresponds to the impact step.

Let us adapt the approaches applied previously to study model mechanisms, for the qualitative and numerical analysis of (2)–(3). Since, in this case, we are dealing with a concrete reaction, let us analyze it in more detail. In particular, let us pay greater attention to the numerical modelling.

Analysis of steady states. Steady states of the surface are determined from the system of algebraic equations [136]

$$P(\theta_o, \theta_{CO}) = 0 \tag{4}$$

$$Q(\theta_o, \theta_{CO}) = 0 \tag{5}$$

From eqn. (5) we obtain

$$\theta_{CO} = \frac{k_2 P_{CO} (1 - \theta_o)}{k_2 P_{CO} + k_{-2} + k_3 \theta_o} \tag{6}$$

$$(1 - \theta_o - \theta_{CO}) = \frac{(k_{-2} + k_3 \theta_o)(1 - \theta_o)}{k_2 P_{CO} + k_{-2} + k_3 \theta_o}$$

After substituting eqn. (6) into eqn. (4), we have

$$\begin{aligned}
 2k_1 P_{O_2} \frac{(k_{-2} + k_3 \theta_o)^2 (1 - \theta_o)^2}{(k_2 P_{CO} + k_{-2} + k_3 \theta_o)^2} &= \theta_o \left(k_4 P_{CO} + 2k_{-1} \theta_o + \right. \\
 &\quad \left. + \frac{k_2 P_{CO} k_3 (1 - \theta_o)}{k_2 P_{CO} + k_{-2} + k_3 \theta_o} \right)
 \end{aligned} \tag{7}$$

Let us write eqn. (7) as $f(\theta_o) = g(\theta_o)$, where $f(\theta_o)$ and $g(\theta_o)$ are the formation and consumption rates for the adsorbed oxygen, represented in Fig. 1. The formation rate $f(\theta_o)$ had an extremum peak, whereas that of consumption $g(\theta_o)$ is monotonic. It is the different character of these curves that provides

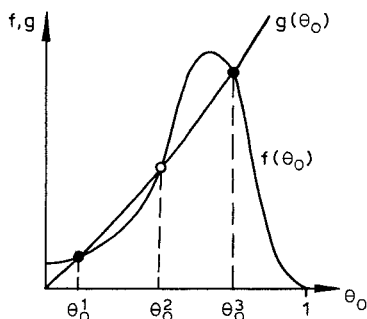


Fig. 1. Dependences of the formation (f) and consumption (g) rates on the concentration of adsorbed oxygen θ_0 for the system (2)-(3).

the possibility of several steady states. The formation rate $f(\theta_0)$ is defined by both P_{O_2} and P_{CO} since carbon monoxide blocks active surface sites. The consumption rate $g(\theta_0)$ is independent of P_{O_2} ; in the chosen scheme the adsorbed oxygen does not react either with gaseous oxygen or with any other form of the adsorbed oxygen.

System (2)-(3) can have only one boundary steady state, i.e. ($\theta_0 = 0$, $\theta_{CO} = 1$) at $k_{-2} = 0$.

We will obtain sufficient conditions for the existence of three solutions for (2)-(3) as has been done for the model adsorption mechanism. Let us demand that, at the point of inflexion θ_0^* for the function $f(\theta_0)$, the condition

$$\begin{aligned} f(\theta_0^*) &= g(\theta_0^*) \\ \frac{df(\theta_0^*)}{d\theta_0} &\geq \frac{dg(\theta_0^*)}{d\theta_0} \end{aligned} \quad (8)$$

will be satisfied. By its physical significance the inequality from (8) is identical to that from (23) in Chap. 5: in the unstable steady state, the derivative of the formation rate for the adsorbed oxygen must be greater than that for its consumption. Condition (8) is similar to the known condition of thermal explosion [137]

$$\frac{dQ_p}{dT} > \frac{dQ_T}{dT}$$

where Q_p and Q_T are the rates of heat release and heat removal, respectively, and T is the temperature.

Let us suggest that the reaction takes place at sufficiently low temperatures and its reversibility can be neglected: $k_{-1} = k_{-2} = 0$. Then from condition (8) we can easily obtain a simple condition for the multiplicity of steady states

$$3k_1 P_{O_2} > 9k_2 P_{CO} \left(1 + 3 \frac{k_2}{k_3} P_{CO} \right) \left(\frac{2}{3} + \frac{k_4}{3k_2} + \frac{k_4}{k_3} P_{CO} \right) \quad (9)$$

whence it is seen that, other conditions being equal, the multiplicity of steady states will be observed at sufficiently low concentrations of CO and high concentration values of O₂. As to the effect of temperature, the constants k_1 , k_2 , and k_4 are independent of temperature (the values of these constants will be given below). Temperature affects only k_3 . Its elevation promotes a multiplicity of steady states. But at sufficiently high temperatures, reaction reversibility cannot be neglected ($E_{-1}, E_{-2} > 0$). In this case new conditions can also be obtained from (8). Since they are cumbersome, we will not represent them here and will only note that by increasing the reversibility, the region for the multiplicity of steady states is reduced.

A simple inequality that is a necessary condition for the multiplicity of steady states is obtained from the mere fact that the $f(\theta_0)$ curve has a point of inflexion. From $f''_{\theta_0}(\theta_0^*) = 0$, we obtain

$$\theta_0^* = \frac{1}{2(3^{1/2})} \left[3^{1/2} - 1 - \frac{k_{-2}}{k_3} (3^{1/2} + 1) \right]$$

and since $\theta_0^* > 0$, it is necessary that the inequality

$$\frac{k_{-2}}{k_3} < \frac{3^{1/2} - 1}{3^{1/2} + 1} \approx 0.227 \quad (10)$$

is fulfilled. This condition is valid at sufficiently weak reversibility of the step for CO adsorption. It is coincident with the necessary condition for the multiplicity of steady states (25) in Chap. 5 obtained for the three-step adsorption mechanism [138]. The addition of the impact step produced no effect on this condition. This is natural since the expression for $f(\theta_0)$ does not contain a constant of the impact step k_4 .

The stability of steady states is analyzed [139] like the investigation performed for the three-step mechanism. In stable steady state, the inequality $dg(\theta_0)/d\theta_0 > df(\theta_0)/d\theta_0$ is fulfilled. In the unstable steady state, the sign of this inequality reverses. It can easily be shown that the unique steady state is always stable. If there are three steady states, the outer are stable and the middle is unstable. It can be suggested that the addition to the three-step adsorption mechanism of the impact step that is linear with respect to the intermediate does not produce any essential changes in the phase pattern of the system. The only difference is that at $k_{-1} = k_{-2} = 0$ the dynamic model corresponding to the two-route mechanism can have only one boundary steady state ($\theta_0 = 0, \theta_{CO} = 1$).

In addition, the existence of the impact step leads to a reduction in the region for the multiplicity of steady states compared with the adsorption mechanism. The impact step is an additional (linear) reaction of the ad-

TABLE 6

Rate constants for elementary reactions of mechanism (1) for the CO oxidation over polycrystalline Pt according to the data of refs. 48 and 49

Number of the reaction (<i>i</i>)	1	-1	2	-2	3	4
E_i (kcal mol ⁻¹)	-3.3 ^a	58.5	0	34	28.75	0
k_i^0	10 ¹⁹	4.16 × 10 ³⁰	1.5 × 10 ²⁰	3.9 × 10 ²⁶	3.14 × 10 ²⁷	2.1 × 10 ²⁰
Dimension of k_i^0	<u>molec.</u>	<u>molec.</u>	<u>molec.</u>	<u>molec.</u>	<u>molec.</u>	<u>molec.</u>
	cm ² s Torr	cm ² s	cm ² s Torr	cm ² s	cm ² s	cm ² s Torr

^aFrom independent adsorption experiments [65].

sorbed oxygen consumption. The contribution of this step is similar to that of the desorption reactions which decrease the concentration of substances adsorbed on the surface.

Modelling of kinetic dependences. Calculation of steady state kinetic dependences according to the model (4)–(5) cannot be performed without knowing the rate constants. Let us use the parameters (Table 6) for the two-route mechanism (1), the complete set of which was first given by Cassuto et al. [49]. The kinetics and mechanism for CO oxidation over polycrystalline platinum were studied [48] using the molecular beam technique.

Steady-state behaviour of the reaction in the space of the parameters ($T \times P_{O_2} \times P_{CO}$) will be characterized by the diagrams of steady states (d.s.s.). These diagrams are the section of this space by the planes $T = \text{const.}$, $P_{O_2} = \text{const.}$, and $P_{CO} = \text{const.}$ D.s.s. are obtained from solutions of (4)–(5), i.e. the steady state kinetic model. The parameters range within $T = 400\text{--}1000\text{ K}$ and P_{O_2} and $P_{CO} = 10^{-9}$ to 10^{-5} Torr.

The region for the multiplicity of steady states in the coordinates $T \times P_{O_2} \times P_{CO}$ is shown in Fig. 2. The same region is represented in various d.s.s. (Fig. 3), characterizing its evolution by varying the respective parameter (T , P_{O_2} , P_{CO}). In all these diagrams the region of multiplicity is rather narrow but extended.

Numerical simulation permits us to identify a region of the parameters with essentially different kinetic characteristics. As an example, let us take the d.s.s. ($T \times P_{CO}$) at $P_{O_2} = 2 \times 10^{-6}$ Torr (Fig. 4). Here we can conventionally select 6 regions (A–F). Region A ($T > 700\text{ K}$): $W(P_{CO})$ has a shape of the curve with saturation and the function $W(T)$ falls with increasing temperature [Fig. 5(a) and (b), respectively]. Region B: the function $W(P_{CO})$ has a maximum peak; $W(T) \cong \text{const.}$ Region C: the maximum peak is observed for the function $W(T)$. Region D: $W(P_{CO})$ is a linear function; $W(T) \cong \text{const.}$ Region E: $W \approx 0$, since $\theta_{CO} \approx 1$. Finally, region F: here the multiplicity of

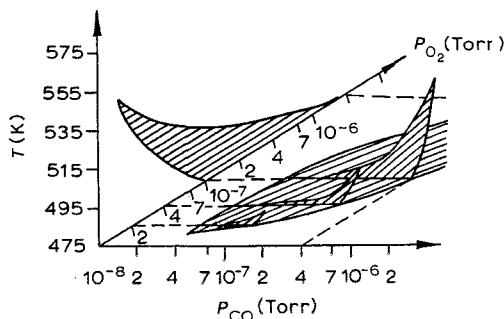


Fig. 2. Region for the multiplicity of steady state in the space $T \times P_{O_2} \times P_{CO}$ for reaction (1) with parameters from ref. 49.

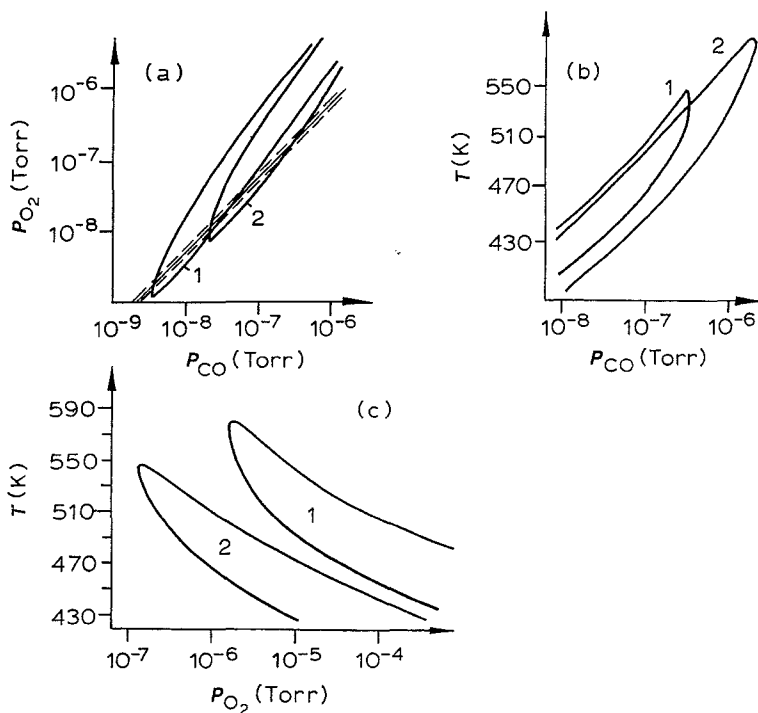


Fig. 3. Regions for the multiplicity of steady states: (a) d.s.s. $P_{O_2} \times P_{CO}$ (1, $T = 475$ K; 2, $T = 500$ K). Broken lines indicate stoichiometric compositions; (b) d.s.s. $T \times P_{CO}$ (1, $P_{O_2} = 2 \times 10^{-7}$; 2, $P_{O_2} = 2 \times 10^{-6}$ Torr); (c) d.s.s. $T \times P_{O_2}$ (1, $P_{CO} = 2 \times 10^{-6}$; 2, $P_{CO} = 2 \times 10^{-7}$ Torr).

steady states is observed. Kinetic functions are unambiguous. The function $W(P_{CO})$ is characterized by the "clockwise" hysteresis [Fig. 5(a)] whereas for $W(P_{O_2})$ and $W(T)$, the hysteresis is "counterclockwise" [Fig. 5(b), (c)].

The regions for the multiplicity of steady states represented in Figs. 2 and 3 were constructed from the numerous solutions of the steady state equation (7) by varying P_{O_2} , P_{CO} , and T within a given range [140]. Later [141], a more efficient computational method for the construction of the boundary for the multiplicity region in the plane of the parameters P_{O_2} and P_{CO} was used. This method makes essential use of the specificity in the dependence of eqn. (7) on P_{O_2} and P_{CO} . Equation (7) can be represented as

$$F(\theta_0) = 0 \quad (11)$$

$$\theta_0 \in [0, 1]$$

where F is the polynomial of the fourth degree such as $F(0) > 0$, $F(1) < 0$.

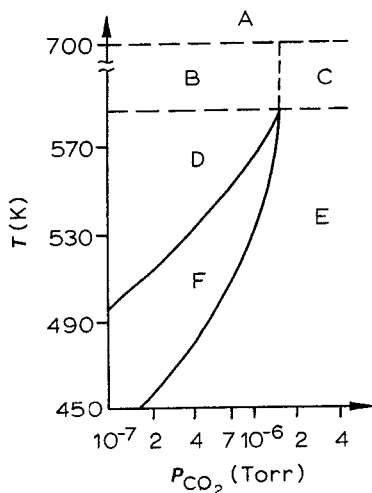


Fig. 4. Regions of various qualitative behaviour for the reaction rate in d.s.s. ($T \times P_{CO_2}$); P_{O_2} constant.

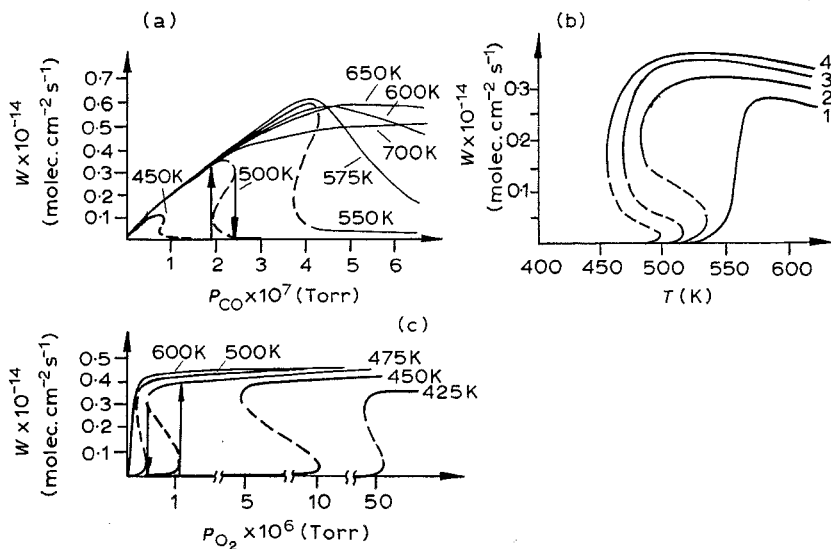


Fig. 5. Dependences of steady-state reaction rate. (a) $W(P_{CO})$ at $P_{O_2} = 1.3 \times 10^{-7}$ Torr; (b) $W(T)$ at $P_{CO} = 2 \times 10^{-7}$ Torr 1, P_{O_2} (Torr) = 1×10^{-7} ; 2, P_{O_2} (Torr) = 2×10^{-7} ; 3, P_{O_2} (Torr) = 4×10^{-7} ; 4, P_{O_2} (Torr) = 7×10^{-7} ; (c) $W(P_{O_2})$ at $P_{CO} = 2.2 \times 10^{-7}$ Torr.

P_{O_2} enters into eqns. (4) linearly, hence knowing θ_0 and P_{CO} , we can find not only θ_{CO} but also P_{O_2}

$$P_{O_2} = \Phi(\theta_0, P_{CO}) \quad (12)$$

If we introduce into our consideration the function [141]

$$G(\theta_0, P_{CO}) = (k_{-2} + k_3\theta_0)(1 - \theta_0)F'(\theta_0) - 2[k_3(1 - \theta_0) - (k_{-2} + k_3\theta_0)]F(\theta_0)$$

which (and it can easily be tested) does not depend on P_{O_2} , the bifurcational curve (the boundary for the multiplicity region) on the plane (P_{O_2}, P_{CO}) is set as (12), where θ_0 is determined from the equation $G(\theta_0, P_{CO}) = 0$ ($P_{CO} > 0$, $0 < \theta_0 < 1$). Hence the required boundary on the plane (P_{O_2}, P_{CO}) is determined as follows. For a fixed value of P_{CO} we solve with respect to θ_0 the equation: $G(\theta_0, P_{CO}) = 0$. From the determined value of θ_0 and a given P_{CO} in accordance with eqn. (12), the value for P_{O_2} will be found.

Calculated data for the set of parameters given in ref. 142 are represented in Fig. 6. In a given pressure range 10^{-8} Torr $\leq P_{O_2}$, $P_{CO} \leq 10^{-6}$ Torr, a multiplicity of steady states is observed at $358 \text{ K} < T < 510 \text{ K}$.

A method of constructing the boundaries for the region of multiplicity of steady states [141] as applied to the CO oxidation over Pt is sure to be of a general character. Methodical strategy of this problem, consisting in obtaining analytical expressions for the boundaries of the multiplicity region, can also be useful for the analysis of the other systems and the other types of critical effect.

Comprehensive interpretation of kinetic curves requires the analysis of

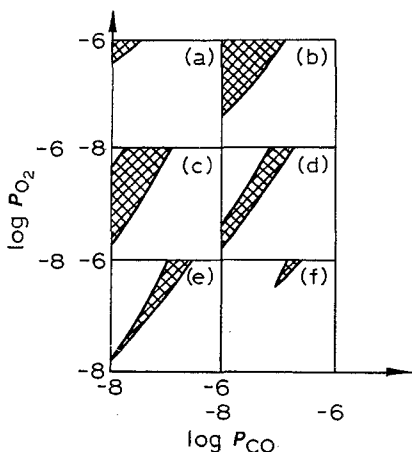


Fig. 6. Bifurcation curves plotted on the $(\log P_{O_2}, \log P_{CO})$ plane. The region for the multiplicity of steady states is hatched. (a) 370 K; (b) 430 K; (c) 440 K; (d) 470 K; (e) 487.1 K; (f) 500 K.

the parametric effect on the steady state composition of surfaces. This effect can also be trivial, i.e. with increasing P_{CO} , θ_{CO} rises whereas θ_{O} falls; with increasing P_{O_2} , θ_{O} increases and θ_{CO} decreases. With increasing temperature, θ_{CO} decreases, whereas θ_{O} passes through its maximum value. It is the decrease of θ_{O} caused by desorption at sufficiently high temperatures that leads to the decrease in $W(T)$ in region A.

An important characteristic for the reaction is the contribution of the adsorption and impact mechanism. A strict determination of their sizes, α_{ads} and α_{im} , can be determined by

$$\alpha_{\text{ads}} = \frac{W_3}{W_3 + W_4}$$

$$\alpha_{\text{im}} = \frac{W_4}{W_3 + W_4}$$

In the region of relatively low values of P_{CO} (region D), the main contribution is made by the impact step $W_4 = k_4 P_{\text{CO}} \theta_{\text{O}}$. Its rate constant does not depend on temperature. Apparently, $W(P_{\text{CO}})$ must be linear.

In regions B and C, the contributions of impact and adsorption mechanisms are commensurate. If, in region B, the temperature is elevated (with P_{CO} remaining unchanged) the values of θ_{CO} and θ_{O} fall. As shown above, the rate of the impact mechanism is temperature independent. As to the adsorption mechanism, the rate constant of step (3) having a high activation energy ($E_3 \approx 29 \text{ kcal mol}^{-1}$ [49]) falls sharply in region B. The rise of $k_3(T)$ compensates the decrease of $\theta_{\text{CO}}(T)$ and $\theta_{\text{O}}(T)$. Therefore the total rate of CO_2 generation is practically temperature independent.

The contribution of the adsorption mechanism increases continuously in region A. Here it dominates despite the fact that θ_{O} and θ_{CO} are low ($\theta_{\text{O}} < 0.1$ and θ_{CO} is at least an order in magnitude lower). It is also ascribed to the increase of $k_3(T)$. A zero order with respect to CO in this region is due to the compensation with increasing P_{CO} : θ_{CO} rises, whereas θ_{O} falls. It must be understood that our suggestions concerning the relative contributions of adsorption and impact mechanisms are valid only for the set of reaction parameters taken from ref. 49. When these parameters (or even the parameters of individual reaction steps) are modified, these suggestions can change markedly.

Thus, in terms of a sufficiently simple two-route mechanism, it is possible to interpret the effects observed by different authors [48, 53, 62, 98]: (1) a jumpwise increase in the reaction rate at definite temperatures; (2) temperature independence of the rate and simultaneously first order with respect to CO at "low" T and P_{CO} ; (3) zero order with respect to CO at "high" T . The model corresponding to the two-route mechanism and using the parameters from ref. 49 predicts the existence of critical effects first discovered by Golchet and White [62] under deep vacuum.

Let us perform a more comprehensive numerical analysis of the steady-

state kinetic dependence for the CO oxidation over Ir(110) and on polycrystalline Pt. These data were obtained by Ivanov et al. on a LEED-240 Varian system at pressures ranging within the range 10^{-9} to 10^{-6} Torr and $T \geq 300$ K [67, 106, 143, 144].

Details of the experiment have been described [77, 92, 106]. The authors examined Ir(110) microfacetted by Ir(111) and a polycrystalline Pt foil by using low-energy electron diffraction (LEED), Auger electron spectroscopy (AES), and thermal desorption (TD).

It is essential that oxygen was contained in subsurface Pt layers, dissolving there with increasing temperature. This oxygen, whose removal is extremely difficult, can affect the constants of surface reactions. For example, the initial sticking coefficient of O_2 on the oxidized sample is $S_{O_2} = 0.05$, whereas for the Ir sample that was not exposed to oxygen we have $S_{O_2} = 0.26$ [78, 106, 142]. Since the literature lacks detailed information, our model does not account for this fact.

As to the oxygen dissolution itself, we will use this process for the further modelling of slow relaxation processes. Under reaction conditions at $T > 450$ K, the oxygen film on the Ir(111) and Pt(111) was disordered [59, 92]. It is this fact that formed the basis for the application of the ideal adsorption layer model. As before, we choose the model (2)–(3) corresponding to the two-route mechanism. Its parameters were determined in special experiments by Ivanov et al. The results have been reported elsewhere [67, 77, 106, 142–144]. Desorption constants were determined by using the thermal desorption method. The same method was used to find the constant k_3 . The only difference was that a layer of co-adsorbed reactants was prepared. The constant k_4 was found according to the initial jump in the rate during the titration of the adsorbed oxygen by CO. Rate constants for the adsorption and impact interactions were calculated from the equation

$$k_1(2, 4) = \frac{S_{O_2}(\text{CO})}{N_z(2\pi mkT_g)^{1/2}} \exp \left\{ - \frac{E_1(2, 4)}{RT} \right\}$$

where $S_{O_2}(\text{CO})$ are the sticking coefficients of gaseous O_2 and CO, N_z is the number of active sites per unit surface ($N_z = 8 \times 10^{14}$ cm^{-2} for Pt and 9×10^{14} cm^{-2} for Ir), m is the molecular mass, k is the Boltzmann constant, and T_g is the gas temperature ($T_g = 298$ K). For the calculations it was also suggested that the reaction parameters (pre-exponential factors, activation energies) do not depend on the surface composition and the limiting coverages with O_2 and CO are the same. The set of the parameters applied is given in Table 7.

Let us perform modelling with the application of just these parameters. Let us first estimate the parametric sensitivity of the steady-state kinetic dependences for CO oxidation over Ir(110) to variations in the rate constant. We will assume that $k_2^0 = k_4^0 = 0.36 \times 10^{21}$ molecules $\text{cm}^2 \text{s}^{-1}$ (the number of CO molecule collisions per unit time on unit surface) and $k_{-2}^0 = 10^{13} \text{s}^{-1}$. The desorption constant of O_2 was not varied. The parameters E_3 , E_4 , and k_3^0

TABLE 7

Parameters of steps in mechanism (1)

Catalyst	k_1^0 , ($\text{cm}^2 \text{molec}^{-1} \text{s}^{-1} \text{Torr}^{-1}$)	$k_2^0 = k_4^0$, ($\text{s}^{-1} \text{Torr}^{-1}$)	E_1, E_2 (kcal mol^{-1})	k_{-1}^0 , ($\text{cm}^2 \text{molec}^{-1} \text{s}^{-1}$)	E_{-1} , (kcal mol^{-1})	k_{-2}^0 , (s^{-1})	E_{-2} (kcal mol^{-1})	k_3^0 , ($\text{cm}^2 \text{molec}^{-1} \text{s}^{-1}$)	E_3 (kcal mol^{-1})	E_4 (kcal mol^{-1})
Ir(110)	0.12×10^{-9} ($S_{\text{O}_2} = 0.26$)	0.4×10^6 ($S_{\text{CO}} = 1$)	0	0.26×10^{-2}	70 ± 5	10^{13}	35	10^{-12} - 10^{-11}	11 ± 1	0.7-1.5
Pt polycryst.	0.25×10^{-9} ($S_{\text{O}_2} = 0.45$)	0.45×10^6 ($S_{\text{CO}} = 1$)	0	0.2×10^{-2}	50 ± 2	10^{13}	35	10^{-12} - 10^{-11}	12 ± 2	0

varied within experimental accuracy: $E = \pm 1 \text{ kcal mol}^{-1}$ and k_3^0 within one order of magnitude. The sticking coefficients of O_2 and CO varied from 0.25 to 0.05 and from 1.0 to 0.5, respectively. CO is desorbed in several states, three for $\text{Ir}(110)$ and two for Pt . But in accordance with ref. 78, the weakly bonded states of CO take practically no part in the reaction. Therefore the value of E_{-2} was varied within the energies of the strongly bonded state: $E_{-2} = 33\text{--}37 \text{ kcal mol}^{-1}$. For platinum, $E_4 = 1 \pm 0.5 \text{ kcal mol}^{-1}$. The respective curves are represented in Fig. 7.

With decreasing sticking coefficients S_{O_2} and S_{CO} , the reaction rate also decreases. A similar effect is also produced by a decrease of k_3^0 . The effect of E_3 variations is largely observed in the low-temperature region, whereas those of E_4 manifest themselves at high temperatures. It must be noted, however, that on the whole the steady state kinetic curves are weakly sensitive to the parameters E_3 , E_4 , and k_3^0 . As seen from Fig. 7, the highest sensitivity is observed in the activation energy of CO desorption. It is in this sense that the CO desorption step can be treated as a decisive one in our complex reaction.

A comparison of the experimental and calculated curves for $\text{Ir}(110)$ (at various $P_{\text{O}_2}/P_{\text{CO}}$ ratios) is given in Fig. 8. A similar comparison is represented in Fig. 9 for polycrystalline platinum. As seen, the calculation and the experiment are in good agreement. It must be emphasized, however, that the initial section of the calculated $W_{\text{CO}_2}(T)$ are steeper than those of the experimental curves. The calculations showed that a better description can be obtained through the application of $E_{-2} = E_{-2}^0 - \alpha \theta_{\text{CO}}^n$, where E_{-2}^0 is the desorption activation energy for strongly bonded CO at $\theta_{\text{CO}} = 0$, and n is an empirical parameter ($n \geq 1$). The effect of partial pressures on the kinetic dependences is illustrated in Figs. 8 and 9. With increasing P_{O_2} , the rate

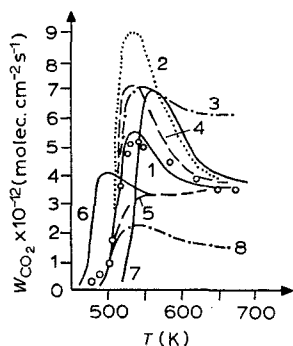


Fig. 7. Calculated curves $W_{\text{CO}_2}(T)$ for CO oxidation over $\text{Ir}(110)$ at $P_{\text{CO}} = 5 \times 10^{-8}$ Torr; $P_{\text{O}_2} = 1.2 \times 10^{-7}$ Torr. Dimensions for k_3^0 and E_i are given in Table 7. 1, $E_{-2} = 35$, $E_3 = 11.5$, $E_4 = 1.5$, $k_3^0 = 5 \times 10^{-12}$, $S_{\text{O}_2} = 0.26$, $S_{\text{CO}} = 1$. For the rest of curves the constants were changed: 2, $E_3 = 10$; 3, $E_4 = 0.5$; 4, $k_3^0 = 10^{-11}$; 5, $k_3^0 = 10^{-12}$; 6, $E_{-2} = 33$; 7, $E_{-2} = 37$; 8, $S_{\text{O}_2} = 0.05$, $S_{\text{CO}} = 0.3$. O, Experimental points.

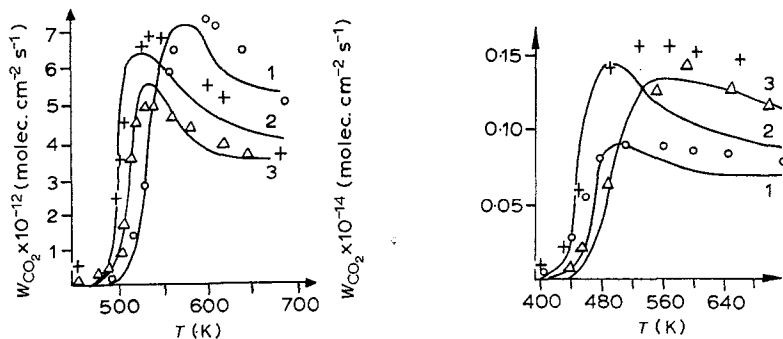


Fig. 8. Calculated and experimental curves $W_{\text{CO}_2}(T)$ for CO oxidation over Ir(110). 1, $P_{\text{O}_2} = 1.2 \times 10^{-7}$, $P_{\text{CO}} = 1 \times 10^{-7}$; 2, $P_{\text{O}_2} = 2.5 \times 10^{-7}$, $P_{\text{CO}} = 0.5 \times 10^{-7}$; 3, $P_{\text{O}_2} = 1.2 \times 10^{-7}$, $P_{\text{CO}} = 0.5 \times 10^{-7}$ Torr. O, Curve 1; +, curve 2; Δ , curve 3.

Fig. 9. Calculated and experimental curves $W_{\text{CO}_2}(T)$ for CO oxidation over polycrystalline Pt. 1, $P_{\text{O}_2} = 0.6 \times 10^{-7}$, $P_{\text{CO}} = 0.5 \times 10^{-7}$; 2, $P_{\text{O}_2} = 1.2 \times 10^{-7}$, $P_{\text{CO}} = 0.5 \times 10^{-7}$; 3, $P_{\text{O}_2} = 0.6 \times 10^{-7}$, $P_{\text{CO}} = 1 \times 10^{-7}$ Torr. O, Curve 1; +, curve 2; Δ , curve 3.

starts to rise in the lower temperature region. The effect of carbon monoxide is just the opposite. But on increasing both P_{O_2} and P_{CO} , the maximum value of the reaction rate increases.

Let us now discuss whether it is possible, on the basis of steady-state experiments, to prefer one of the two sets of parameters for reaction steps from Table 8. Figure 10(a) represents experimental data from ref. 48. The calculated curves for the same conditions are also given. The calculation was carried out with both sets of parameters* [49,142] (see Table 8). Figure 10(b) represents experimental data from ref. 142. The calculated curves are presented plotted by using both parametric sets. In all cases the discrepancy between experiment and calculation is within experimental accuracy. It can only be said that, with the application of the parameters from ref. 49, the kinetic curves have greater parametric sensitivity to $P_{\text{O}_2}/P_{\text{CO}}$. There is, however, an essential difference. With the parameters from ref. 49, the steady-state concentration θ_0 in the high-temperature region is an order in magnitude lower than with the application of the other parameters (Table 7). The calculation using the model with just these parameters produces good reproducibility (Fig. 11) for the θ_0 values measured by using AES over Ir(110). Unfortunately, such measurements have not been made for polycrystalline Pt.

The comparison of the parameters from these two sets shows that an essential difference is observed only in the constant k_3 : k_3^0 differs by more

* In one of the parametric sets the adsorption constant of O_2 is given as $k_1 = AT^{-1/2}$ as suggested in ref. 49.

TABLE 8

Parameters of the steps for the CO oxidation reaction over polycrystalline platinum

Parameters	Ref. 142	Ref. 49
k_1^0 (molec. cm ⁻² s ⁻¹ Torr ⁻¹)	1.62×10^{20}	$k_1 = 6.2 \times 10^{21}/T^{3/2}$ ($T < 750$ K)
E_1 (kcal mol ⁻¹)	0	
k_{-1}^0 (molec. cm ⁻² s ⁻¹)	0.13×10^{28}	0.42×10^{31}
E_{-1} (kcal mol ⁻¹)	50	58
k_2^0 (molec. cm ⁻² s ⁻¹ Torr ⁻¹)	0.36×10^{21}	0.15×10^{21}
k_{-2}^0 (molec. cm ⁻² s ⁻¹)	0.8×10^{28}	0.39×10^{27}
E_{-2} (kcal mol ⁻¹)	35	34
k_3^0 (molec. cm ⁻² s ⁻¹)	0.64×10^{19}	0.314×10^{28}
E_3 (kcal mol ⁻¹)	11	29
k^0 (molec. cm ⁻² s ⁻¹ Torr ⁻¹)	0.36×10^{21}	0.21×10^{21}

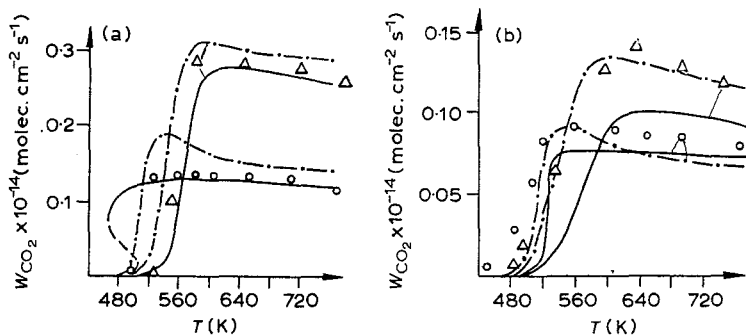


Fig. 10. Comparison of calculated and experimental curves $W_{\text{CO}_2}(T)$ for CO oxidation over polycrystalline Pt. 1 (—), calculation using constants from ref. 49; 2 (---), calculation using constants from Table 7. (a) For experimental data [48] $P_{\text{O}_2} = 2.26 \times 10^{-7}$; 3(○), $P_{\text{CO}} = 0.74 \times 10^{-7}$; 4(Δ), $P_{\text{CO}} = 2.19 \times 10^{-7}$ Torr. (b) For experimental data [142] $P_{\text{O}_2} = 0.6 \times 10^{-7}$; 3'(○), $P_{\text{CO}} = 0.5 \times 10^{-7}$; 4'(Δ), $P_{\text{CO}} = 1 \times 10^{-7}$ Torr.

than 8 orders of magnitude and E_3 is 18 kcal mol⁻¹ higher. In the above discussion of the interaction between various adsorbed substances, we have mentioned that the literature reports on the two groups of k_3^0 and E_3 parameters differ greatly. For example, k_3^0 [49] is close to the value obtained by using the transition state method. But the value obtained [112] from the results of isothermal titration of the adsorbed CO is lower ($k_3^0 = 0.12 \times 10^{20}$ molecules cm⁻²s⁻¹ = 1.87×10^{-11} cm²molecules⁻¹s⁻¹ at $N_x = 8 \times 10^{14}$ molecules cm⁻²). A close value was obtained [78] according to the data for the thermal desorption of the mixed co-adsorbed layer. We must stress a significant fact: Bonzel and Barton [112] and Ivanov et al. [106] found values for k_3 in special experiments. As to ref. 49, the authors obtained k_3 from the

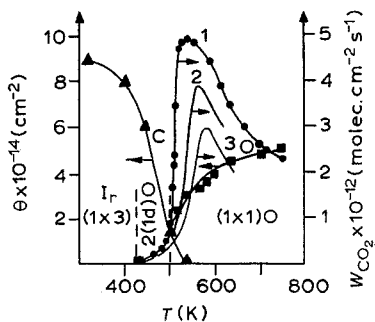


Fig. 11. Temperature dependence of reactant concentrations and reaction rate over Ir(110). $P_{\text{CO}} = 5 \times 10^{-8}$ and $P_{\text{O}_2} = 1.2 \times 10^{-7}$ Torr. 1, W_{CO_2} under steady-state conditions; 2, 3, W_{CO_2} on heating catalyst at $v = 2$ and 4 K s^{-1} , respectively. C and O = relative variations in the altitude of Auger peaks for carbon and oxygen under steady-state conditions [78].

solution of the inverse kinetic problem. The fact that k_3^0 is slightly lower than the value obtained by using the transition state method was ascribed by Ivanov to the low value of the transition coefficient κ [48]. Zhdanov and Zamaraev [145] believe that no experiment has so far been carried out on the basis of which this constant could be determined correctly, i.e. no experiment has been reported in which the interaction rate of O_2 and CO would be determined at different temperatures but at the fixed surface composition. Note that the realization of such an experiment is extremely difficult. In our opinion, the enigma of the constant k_3 consists in the fact that the interaction of O_2 with CO is a complex process. Apparently, the adsorption and the impact routes are its specific manifestations. It is also possible that the parameters of this process sharply change with certain compositions of gas mixture and temperature. It is this change in the parameters that was emphasized by Campbell, et al. [56].

Calculation according to the group of parameters [142] with greatly differing k_3^0 and E_3 values leads to the other suggestions about the contributions of impact and adsorption mechanisms. With decreasing E_3 in the region of low temperatures (up to 550 K) and low partial pressures the predominant contribution is made by the adsorption mechanism. The calculated contribution of adsorption and impact mechanisms to the overall rate of the reaction over Ir(110) are represented in Fig. 12. Kinetic curves for these mechanisms calculated according to the concentrations θ_{O} and θ_{CO} measured by the AES method are also given. When the total pressure rises but the ratio $P_{\text{O}_2}/P_{\text{CO}}$ is constant, the contribution of the adsorption mechanism decreases (curves 1,2 and 6,7 in Fig. 12). The kinetic curves shift towards high temperatures.

It can be stated that the two-route mechanism and its respective kinetic model at given temperatures ($T > 450 \text{ K}$) and partial pressures resulting in the disordered oxygen layer are a good approximation of the description of

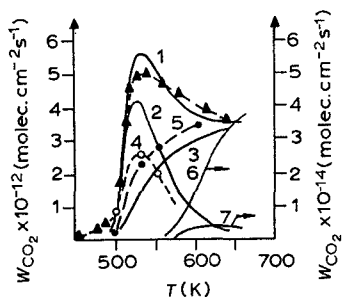


Fig. 12. Temperature dependence $W_{\text{CO}_2}(T)$ for CO oxidation over Ir(110) at $P_{\text{O}_2} = 1.2 \times 10^{-7}$ and $P_{\text{CO}} = 5 \times 10^{-8}$ Torr. 1, Overall rate (calculated and experimental); 2, 3 rate calculated according to L-H and E-R mechanisms, respectively; 4, 5 experimental rate according to L-H and E-R, mechanisms, respectively; 6, 7 calculated curves (overall and L-H, respectively) of $W_{\text{CO}_2}(T) \times 10^{-14}$ molecules $\text{cm}^{-2}\text{s}^{-1}$ at $P_{\text{O}_2} = 1.2 \times 10^{-5}$ and $P_{\text{CO}} = 5 \times 10^{-6}$ Torr.

the kinetic curves [67, 106]. It is essential that we can obtain a kinetic model for complex reactions through the application of our knowledge about the regularities of individual steps examined in special independent experiments. We believe it is a very promising method for other cases as well since this assembling corresponds to the very sense of modelling.

3. Dynamic studies of CO oxidation

Let us perform this study like that carried out for the adsorption mechanism. We will analyze time variations in the solutions of the unsteady-state model (2)–(3). Typical phase patterns are represented in Fig. 13. The heavy closed lines are two isochrones [in this case they are geometric sites of the

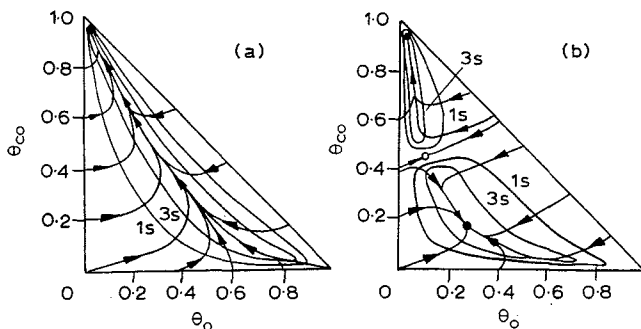


Fig. 13. Reaction phase patterns. $P_{\text{O}_2} = 2.3 \times 10^{-7}$ and $P_{\text{CO}} = 2.2 \times 10^{-7}$ Torr. (a) Unique steady state, $T = 450$ K; (b) three steady states, $T = 490$ K.

points where the system (2)–(3) enters after a certain given time period (1 and 3 s), starting from the initial conditions that correspond to the faces of the phase pattern].

A numerical analysis of the model (2)–(3) shows that, as for the adsorption mechanism, two time scales (fast and slow) exist. The fast scale is typical for the initial segment of the trajectory and the slow scale characterizes motion to the steady state near a certain general trajectory ("mainstream").

The reason for the time separation is the sharp difference in reaction parameters. For example, at low temperatures we have $k_3 \ll k_1 P_{O_2}, k_2 P_{CO}, k_4 P_{CO}$. But starting from a certain temperature (above ~ 500 K in our region) we may obtain $k_3 \gg k_1 P_{O_2}, k_2 P_{CO}, k_4 P_{CO}$.

In numerical experiments, slow relaxation is distinctly observed if the trajectory approaches the unstable steady state. The system rapidly enters its neighbourhood (after ~ 1 s) and then relatively slowly (during ~ 100 s) moves toward its stable steady state. This phenomenon has been described for the three-step adsorption mechanism.

To interpret differences in the relaxation times, it is necessary to start from the analysis of eigenvalues of the matrix for (2)–(3) linearized in the neighbourhood of the steady state (indicated by *). This matrix corresponds to the characteristic equation

$$\begin{aligned} \lambda^2 + \{4k_1 P_{O_2}(1 - \theta_0^* - \theta_{CO}^*) + 4k_{-1}\theta_0^* + k_3(\theta_0^* + \theta_{CO}^*) + \\ + P_{CO}(k_2 + k_4) + k_{-2}\}\lambda + \theta_0^* \{4[k_{-1}(k_2 P_{CO} + k_{-2}) + \\ + k_1 P_{O_2}(k_3 + k_{-2})] + k_3 P_{CO}(k_4 - k_2)\} - 4k_3(k_1 P_{O_2} - \\ - k_{-1})(\theta_0^*)^2 + \theta_{CO}^* k_3(k_2 P_{CO} + k_{-2}) - 4k_1 P_{O_2}(k_3 + k_{-2}) + \\ + 4k_1 k_3 P_{O_2}(\theta_{CO}^*)^2 + k_4 P_{CO}(k_2 P_{CO} + k_{-2}) + 4k_1 k_{-2} P_{O_2} = 0 \end{aligned} \quad (13)$$

The relaxation diagram characterizing the temperature dependence of the roots for the characteristic equation (eigenvalues) is shown in Fig. 14. The temperature dependence of the time required to achieve the steady state is shown in Fig. 15. This time is interpreted as that required for the complete entering of the trajectory into the steady-state ε -neighbourhood (see Chap. 5, Sect. 4). The temperature variation is assumed to be stepwise (see discussion below).

Taken together, the plots from Figs. 14 and 15 are very informative. For example, when going along the two stable branches of the steady-state rate (Fig. 16) far from bifurcations, we can observe no less than a four-fold difference in the eigenvalues of λ . This corresponds to the fact that, in numerical experiments, the difference in relaxation times is also observed in the case when the steady state is unique. Values of λ for the stable branches also differ: for the lower branch, 1, the absolute value of λ is much smaller than for the upper branch 3. A similar difference is also observed in the times to achieve steady states. When going along branch 1, this time amounts to

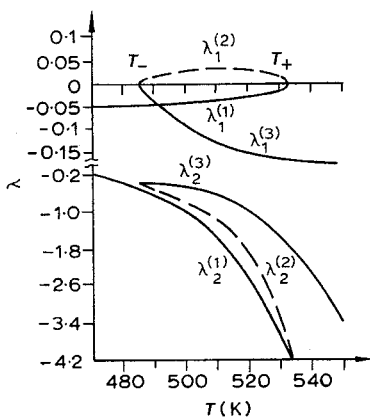


Fig. 14. Temperature dependence of the roots for the characteristic equation (13).

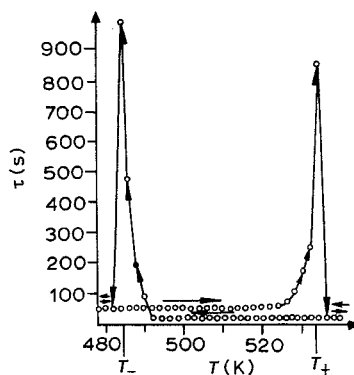


Fig. 15. Time to achieve steady-state reaction rate values as a function of gradual stepwise temperature variation.

about 1 min whereas for branch 3 we have $\tau < 20$ s. This law is natural since, with increasing steady state rate, the relaxation time drops.

Qualitatively, different dependences are observed near the bifurcation points T_+ and T_- (Fig. 16). When approaching T_+ and T_- , the absolute values of $\lambda_1^{(1)}$ and $\lambda_1^{(2)}$ monotonously decrease (at the bifurcation point $\lambda_1 = 0$). Near the bifurcation points, the relaxation time rises sharply. Passing T_+ and T_- is accompanied by long induction periods of the "ignition" and "quenching" (Fig. 17, curves 2 and 4). Hence the relaxation diagram can give us information only about the "ordinary" separation of times associated with difference in parameters of the complex reaction. Eigenvalues are only local dynamic characteristics for the system. To predict the "critical retar-

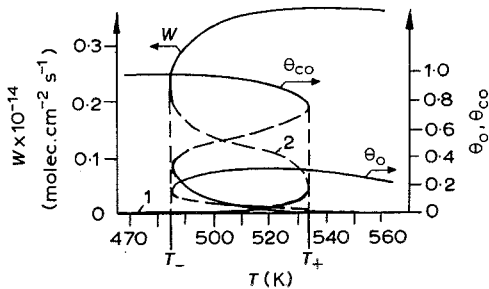


Fig. 16. $W(T)$, $\theta_0(T)$, $\theta_{CO}(T)$ at $P_{O_2} = 2.3 \times 10^{-7}$ and $P_{CO} = 2.2 \times 10^{-7}$ Torr. 1, 3, Branches of stable steady-state reaction rates; 2, unstable values.

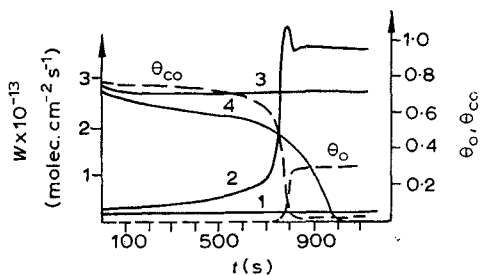


Fig. 17. Reaction rate relaxation at stepwise temperature changes. 1, 530 K to 532 K; 2, 532 K to 534 K; 3, 488 K to 486 K; 4, 486 K to 484 K. Broken curves: θ_O and θ_{CO} for 532 K to 534 K.

dation" observed in the neighbourhood of bifurcation points, one must know the topology of the phase pattern as a whole and obtain the global characteristics. It must be noted that, strictly speaking, the value of λ cannot be used to characterize relaxations far from the steady state. For example, at high temperatures when the reaction constants have sufficiently high values and the steady state is stable, we can have a region of initial conditions, starting from which slow transient processes are observed. A phase pattern of the system at $T = 550$ K, when the constant k_3 is much higher than the rest of the rate constants, is represented in Fig. 18(d). Therefore the reaction of adsorbed O_2 and CO takes place at a high rate and the surface is practically free. Phase trajectories rapidly enter into the region between the null

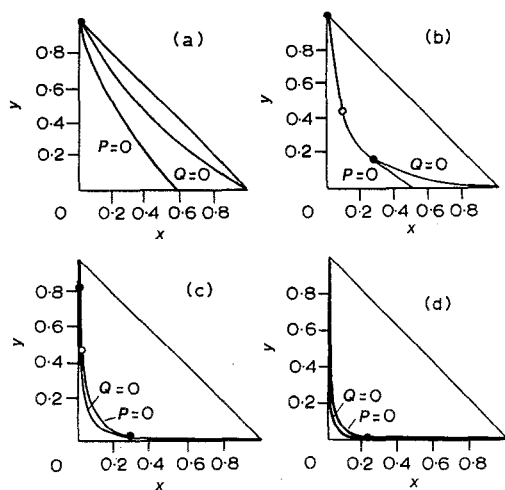


Fig. 18. Null clines and steady states of reaction (1) at $P_{O_2} = 2.3 \times 10^{-7}$ and $P_{CO} = 2.2 \times 10^{-7}$ Torr. $T =$ (a) 450; (b) 490; (c) 530; (d) 550 K.

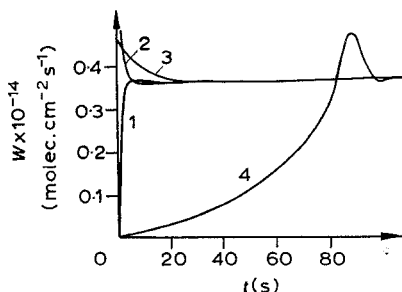


Fig. 19. Relaxation of reaction rate towards the unique steady state from different initial conditions (θ_0, θ_{CO}) for the case from Fig. 18(d). $(\theta_0, \theta_{CO}) = (0, 0), (0.5, 0.5), (1, 0)$, and $(0, 1)$ for curves 1–4, respectively.

clines (into the "mainstream") and can move sufficiently slowly along it. Curve 4 in Fig. 19 illustrates this kind of behaviour.

Special lines (separatrices) separate the regions of the steady-state attraction. The analysis shows that, in our parametric range, the attraction region of the steady state is the smaller the lower is the reaction rate. With increasing temperature from T_- to T_+ , this region sharply reduces (from ~ 30 down to $\sim 10\%$ of the simplex area). It is known that the real experiment is characterized by fluctuations of the surface state, temperature, and gas phase composition. It is this that is responsible for the fact that the region for the multiplicity of steady states predicted by the deterministic model can degenerate into that with an unique steady state possessing high parametric sensitivity. This fact is one of the obstacles for the experimental determination of the multiplicity of steady states.

Let us analyze the transient regimes corresponding to different methods of obtaining parametric (e.g. temperature) dependences of the steady state rate. They are (a) a step by step method when, under the stepwise variation of the parameter, the steady state of the catalyst from the previous experiment is the initial state for the next experimental run (as a rule, it is a common practice in experiments) and (b) an "everything from the very beginning" method when, before every change of a certain parameter, the catalyst is returned to some initial state (e.g. its surface is cleaned of the previously adsorbed substances). The phase pattern of the reaction (Fig. 20) illustrates the states of system (2)–(3) under stepwise temperature variation. Points show stable steady states with nearly corresponding temperatures. Two trajectories are represented: (1) when the temperature rises from 533 to 534 K ("ignition") and (2) when the temperature decreases from 485 to 484 K ("quenching"). Marks on the phase trajectories correspond to that composition (θ_0, θ_{CO}) which are characteristic for the surface at an adjacent instant of time.

Let us emphasize the following peculiarities of transient regimes.

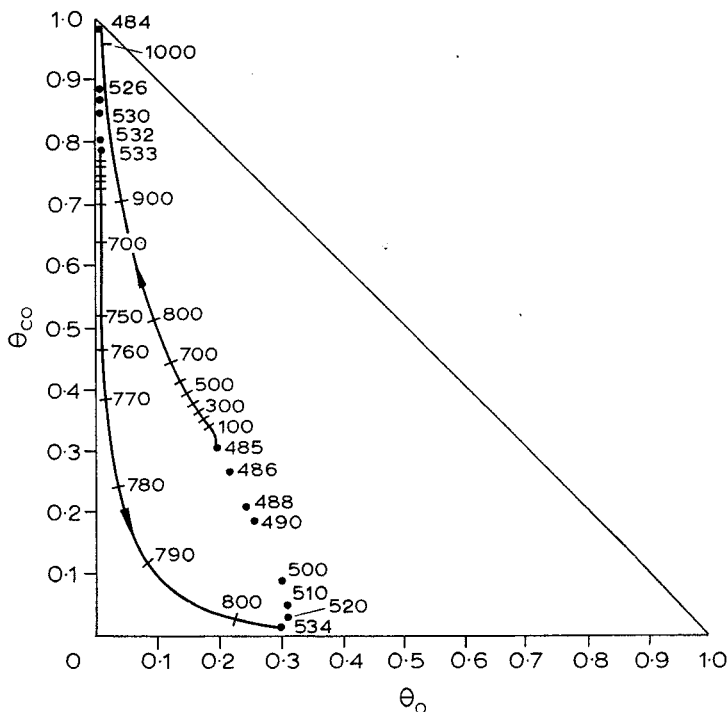


Fig. 20. Variation of steady states with temperature on the phase pattern $P_{O_2} = 2.3 \times 10^{-7}$, $P_{CO} = 2.2 \times 10^{-7}$ Torr. Points: stable steady states at given temperatures (K). Lines: system trajectories at stepwise temperature variations (533 to 534 K and 485 to 484 K).

(1) With increasing temperature and passing through the bifurcation point T_+ , the transient regime of the reaction rate has an "overflight" through its steady state value (see Fig. 17, curve 2). The reason is that the phase trajectory goes through the region of "mean" θ_O and θ_{CO} , ensuring a high value of the component $k_3\theta_O\theta_{CO}$. A point of the phase pattern accounting for the maximum reaction rate is localized far from the steady-state point. It is this fact that can be a base for the advantage of the unsteady-state performance of the reaction process.

(2) With decreasing temperature, passing through the bifurcation point T_- , the reaction rate changes more slowly than the surface composition. The point is that the oxygen deficiency of the surface (θ_O) is partly compensated by the rising CO content (θ_{CO}) and the rate of CO_2 generation ($k_3\theta_O\theta_{CO}$) remains practically unchanged.

(3) With step-by-step motion along the stable branches 1 and 3, the relaxation time must depend on the step value ΔT . For example, with increasing (decreasing) ΔT , the distance on the phase pattern that must be passed by the

system increases (decreases) on the one hand, but, on the other hand, the reaction parameters increase (decrease). These factors can compensate each other and the relaxation time remains practically unchanged.

But as has already been noted, in the neighbourhood of the bifurcation point, the closer the parameter is to the bifurcation value, the longer is the relaxation process ("critical retardation").

Transient regimes obtained by the "everything from the very beginning" method are essentially dependent on the initial conditions. Various regions of the simplex (V_1 , V_2 , and V_3) are represented in Fig. 21. Their borders are separatrices of steady states, "saddles-nodes" S_1 and S_2 that arise at bifurcation values T_- and T_+ , respectively. If the motion begins from a point belonging to the region V_3 (where the surface content of oxygen is high), then with increasing temperature the jump to the "upper" steady state branch will have already taken place at T_- .

The steady state kinetic curve has no hysteresis [Fig. 22(a)]. The temperature dependence of the relaxation time is represented in Fig. 23(a). In the case in which motion begins from a point in the region V_1 (the CO surface coverage is high), with decreasing temperature, the jump to the "lower" steady state branch will have already taken place at T_+ [Fig. 22(b)]. Here, too, no hysteresis will be observed. The temperature dependence of the relaxation time is given in Fig. 23(b).

However, if the initial state is the point lying in the region V_2 , the plots are of a qualitatively different character. The point is that, at temperatures ranging within T_- , T_+ , the saddle unstable point moves in the region V_2 from S_1 to S_2 . Finally, at some T' it appears that the trajectory starting from the initial state will enter into this unstable point. The value of T' depends on the initial conditions.

If the temperature is in the neighbourhood of T' (above or below), slow relaxations are observed. They occur due to the existence of the trajectory

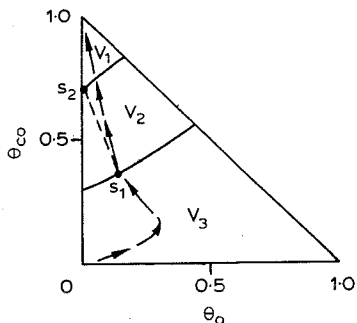


Fig. 21. Subdivision of reaction (1) simplex into subsets. With temperature variation, the regions V_1 and V_3 contain stable steady states and that of V_2 an unstable steady state (at temperatures ranging from T_- to T_+).

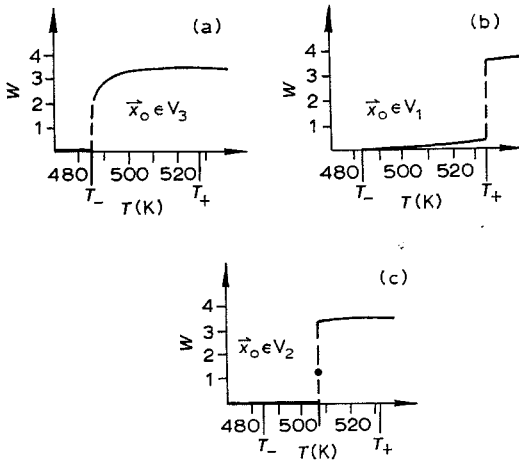


Fig. 22. Temperature dependence of steady-state reaction rate $W(T)$ obtained by the "every time from the very beginning" method. (a) $(\theta_0^{(0)}, \theta_{CO}^{(0)}) \in V_3$; (b) $(\theta_0^{(0)}, \theta_{CO}^{(0)}) \in V_1$; (c) $(\theta_0^{(0)}, \theta_{CO}^{(0)}) \in V_2$.

going from the unstable to the stable steady state. It is interesting that at $T = T'$, the relaxation time is finite. The proper dependences (steady- and unsteady-state) are represented in Figs. 22(c) and 23(c). It has already been noted that the general theory of slow relaxations used as a basis for their classification as been suggested fairly recently by Gorban' et al. [146-149].

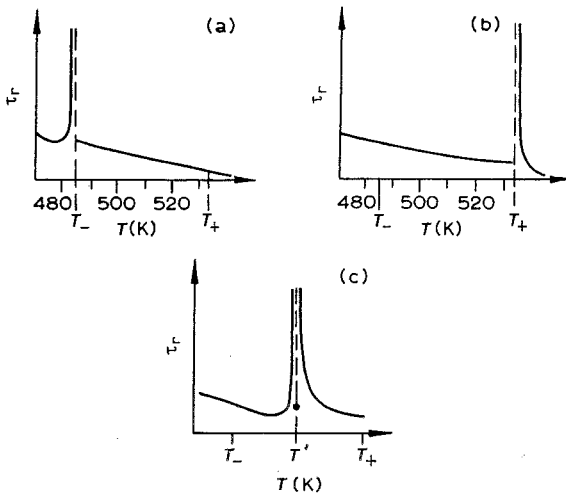


Fig. 23. Temperature dependence of relaxation time $\tau_3(t)$ corresponding to Fig. 22.

Let us emphasize that the "everything from the beginning" procedure cannot provide a hysteresis on the steady-state curves, and only a jump in the reaction rate is realized. Typical unsteady-state plots for the case in which the initial state is specified ($\theta_o = \theta_{co} = 0$) are represented in Fig. 24. In this case there are curves characterized by slow relaxation.

The conditions of kinetic experiments can essentially affect the observed steady- and unsteady-state dependences. For example, in real experiments the observation time is always limited. Hence, in the region of slow relaxations, it can lead to the fact that hysteresis will also be observed in the case when the steady state is unique.

We believe it is this kind of distortion in the kinetic dependences that were observed in refs. 77 and 150. For example, a discrepancy was for the temperature dependence of the reaction rate when the temperature was gradually increased, decreased, and then increased again ($P_{O_2} = 3 \times 10^{-7}$,

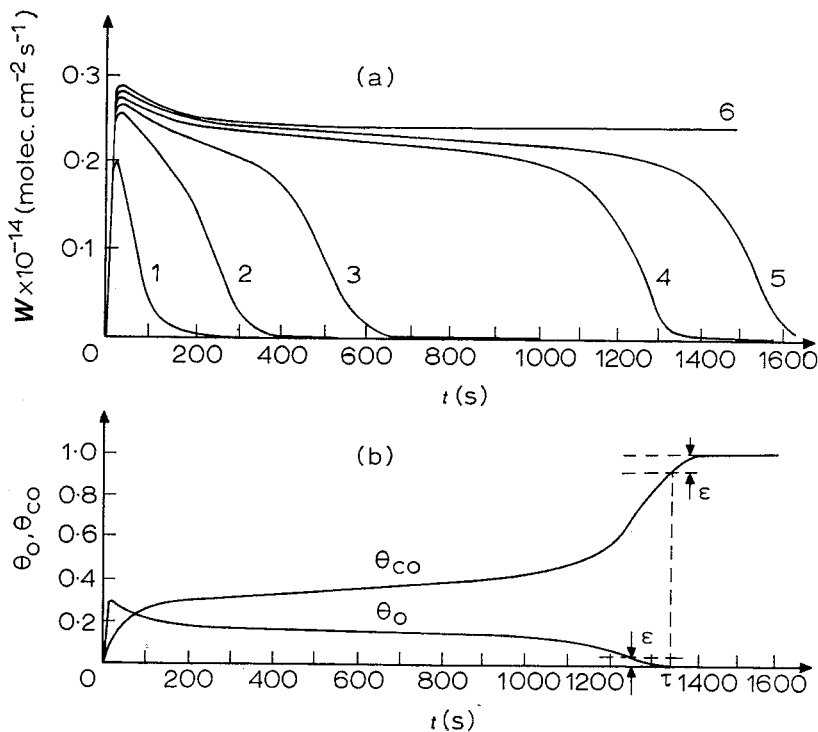


Fig. 24. (a) Relaxation of reaction rate (1) with rate coefficients from ref. 49 when moving from the initial state $\theta_o = 0$, $\theta_{co} = 0$. $P_{O_2} = 2.3 \times 10^{-7}$, $P_{CO} = 2.2 \times 10^{-7}$ Torr. $T = 1$, 450 K; 2, 480 K; 3, 483 K; 4, 484 K; 5, 484.2 K; 6, 484.4 K. (b) Variations in surface coverages θ_o and θ_{co} at $T = 484$ K.

$P_{\text{CO}} = 5 \times 10^{-8}$ Torr). But with a considerable rise in the exposure time, at every temperature point (starting from 5 up to 30–50 min), a slow relaxation was observed [77] from the upper (“metastable”) branch of the kinetic curve to its lower branch where the reaction rate is extremely low. Thus hysteresis peculiarities disappear.

By increasing and decreasing the temperature, relaxation times can differ drastically. This has been proved by experiment [77]. For example, when going from the low-temperature (< 470 K) region to high temperatures (> 490 K), the relaxation time is low (3–5 min). But the reverse transition can be as high as 50 min. It is interesting that the relaxation times for reaction rates and the concentrations of intermediates measured by Auger spectroscopy, which provides the sum of the concentration of substances including that in the subsurface layer, can differ greatly (1 and ~ 20 min, respectively). Numerical analysis shows that the model also gives a low relaxation time (3–5 min) when we go to the high-temperature region (Fig. 25, curve 1). As to the back transition, its calculated time is considerably higher (~ 30 min). Here we move in the region where slow relaxations do exist (Fig. 25, curve 2). Their theoretical study has already been given.

The model also shows the discrepancy in relaxation times for the reaction rate and the concentrations of the intermediates. With decreasing temperature, the coverage θ_0 falls, whereas θ_{CO} rises. They compensate each other and in this temperature range* the rate of CO_2 generation remains unchanged over a considerably long period of time (10–15 min). It is suggested that the non-linear kinetic model permits us to interpret qualitatively the fact of time separation. In addition, it provides a reasonable quantitative estimate for the slow relaxation time (30 out of 50 min). To improve this estimate, the model must take into consideration “side” (Temkin term) proces-

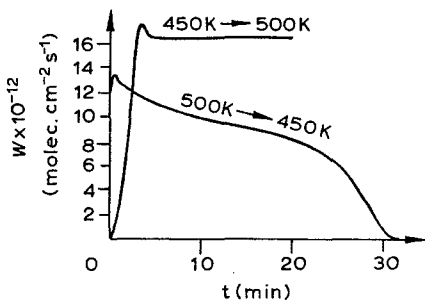


Fig. 25. Relaxation processes to steady states of mechanism (2)–(3) with rate coefficients from Table 7 at stepwise temperature changes ($P_{\text{O}_2} = 3 \times 10^{-7}$, $P_{\text{CO}} = 5 \times 10^{-8}$ Torr).

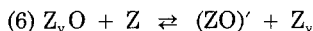
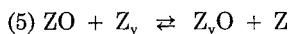
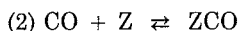
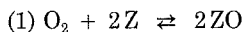
* In this temperature range the adsorption mechanism dominates provided that the parameters of the reaction steps correspond to those from ref. 142.

ses, primarily oxygen diffusion into the catalyst bulk. The importance of taking into account oxygen diffusion also results from the diffraction data [143]. Let us carry out a numerical analysis of two models accounting for this diffusion: (1) a simplified "mechanism" model in which the oxygen exchange between surface and bulk is modelled by the exchange steps, and (2) a diffusion model where oxygen diffusion into the bulk is regulated by Fick's law.

Let us assume that the direct participation of dissolved oxygen in the reaction is insignificant. As a simplifying assumption, we will not take into consideration the dependence of surface reaction parameters on the composition of catalyst bulk; the data about these dependences are still limited in number.

Let us characterize the models and some calculations performed using them.

(1) *The "mechanism" model.* This corresponds to the totality of steps.



where Z_v are active sites in the catalyst bulk, Z_vO is the oxygen dissolved in the catalyst, and $(\text{ZO})'$ is the unreactive surface oxygen.

This mechanism differs from the commonly accepted two-route mechanism in steps (5) and (6) which account for oxygen exchange between surface and bulk. During step (6) an unreactive surface compound of oxygen is formed.

Numerical analysis performed with various rate coefficients for exchange steps (5) and (6) leads to the natural conclusions

(a) by decreasing the rate constants for exchange reactions of step (5), the relaxation time rises and

(b) with increasing rate constant for unreactive $(\text{ZO})'$ formation, the total concentration of working active surface sites falls and the steady-state of CO_2 formation decreases.

(2) *Diffusion model.* A mathematical model accounting for the diffusion of one of the adsorbed substances (oxygen) into the catalyst bulk can be written as

$$\frac{\partial C}{\partial t} = \frac{D}{L^2} \frac{\partial^2 C}{\partial \xi^2}$$

$$t = 0: \theta_0 = \theta_0^{(0)}, \theta_{\text{CO}} = \theta_{\text{CO}}^{(0)}, C = C_0(\xi)$$

$$\begin{aligned} \xi = 0: \frac{\partial C}{\partial \xi} &= 0 \\ \xi = 1: C &= \frac{C_z}{C_v} H \theta_0 \\ \frac{d\theta_0}{dt} &= P(\theta_0, \theta_{CO}) - \frac{DC_v}{C_z L} \left[\frac{\partial C}{\partial \xi} \right]_{\xi=1} \\ \frac{d\theta_{CO}}{dt} &= Q(\theta_0, \theta_{CO}) \end{aligned} \quad (14)$$

where ξ is the dimensionless coordinate, $C(t, \xi)$ is the dimensionless concentration of the diffusing substance Z_vO in the catalyst volume, D is the diffusion coefficient of Z_vO in the catalyst volume (cm^2s^{-1}), L is the thickness of the layer in which diffusion takes place (cm), C_z is the specific number of active surface sites on catalyst (molecules cm^{-2}), C_v is the maximum possible number of Z_vO particles per unit volume (molecules cm^{-3}), H is the dissolution coefficient of adsorbed oxygen in the catalyst volume (cm^{-1}), and $P(\theta_0, \theta_{CO})$ and $Q(\theta_0, \theta_{CO})$ are the kinetic functions (2) and (3) corresponding to mechanism (1).

Models of type (4) have been formulated [151–153] and used for the analysis of some concrete processes [see, for example, ref. 154 where the kinetic dependence $P(\theta_0)$ was represented by a linear function]. Taking into account oxygen diffusion into the catalyst volume by using model (14) does not change the steady states of the catalyst surface compared with model (2)–(3). But the relaxation properties of these models are essentially different. The numerical algorithm developed by Makhotkin was used for the calculations. Discretization of the spatial variable was applied to go from the model in partial derivatives to the system of ordinary differential equations. For details of this algorithm, see ref. 155.

The diffusion coefficient was calculated from

$$\begin{aligned} D &= D_0 \exp \left\{ - \frac{E}{RT} \right\} \\ &= 10^{-2} \exp \left\{ - \frac{20000}{RT} \right\} \text{cm}^2\text{s}^{-1} \end{aligned}$$

Numerical experiments show that the effect of diffusion on the unsteady-state behaviour can be quite different. This effect depends on various factors, in particular the initial composition of catalyst surface and bulk, their steady states and the position of the region for slow relaxations that are of kinetic origin.

For example, if the bulk concentration of oxygen is low (or simply lower than its steady-state value), the movement along the phase trajectory towards the increasing concentrations of surface oxygen is retarded by diffusion. As one goes towards the decreasing concentrations, the movement is

accelerated by diffusion. But if the volume concentration of oxygen is sufficiently high, diffusion exerts quite the opposite effect. Diffusion transforms the phase trajectory so that it can come into the region of slow relaxations. Finally, diffusion can also affect the attraction region of the steady-state point and its type.

The results of the calculations using the diffusion model are illustrated in Fig. 26. The initial conditions were: $\theta_0^{(0)} = 0.5$; $\theta_{CO}^{(0)} = 0.5$; $C_0(\xi) = 0$, i.e. at first oxygen is not present in the bulk.

At $D \rightarrow 0$ ($D_0 \sim 10^{-4}$) the phase trajectories of eqn. (14) coincide with those calculated according to the system (2)–(3) without taking into account diffusion (broken curves AC_1 and AC_2). At $T = 540$ K, the system relaxes to its steady state C_1 within approximately 30 s; at $T = 400$ K, it achieves its steady state C_2 at approximately 300 s. At sufficiently high diffusion coefficients ($D_0 = 10$), oxygen diffuses into the catalyst bulk at a fast rate (approximately 2 s) and the system (at $T = 540$ K) enters the region of slow relaxation (point B on ABC_1). The phase trajectories will now differ from those calculated for the corresponding lumped system. The steady state C_1 is achieved at approximately 700 s instead of 30 s if diffusion is neglected. Phase trajectories BC_1 in the upper part of Fig. 26 illustrate the motion from the point B at $D \rightarrow 0$ ($D_0 = 10^{-4}$) and sufficiently high D ($D_0 = 10$).

At $T = 400$ K, diffusion affects the initial section of the trajectory (accelerates the motion) and exerts practically no effect on the neighbouring region when the concentration of surface oxygen, O_{ads} , varies only slightly.

If the time of a slow relaxation process observed for kinetic curves [77] with decreasing temperature are calculated using the diffusion model, we will obtain a value that is close to that measured by experiment (~ 50 min).

Note that the calculation in which diffusion is not taken into account gives a poorer estimate (~ 30 min). Hence taking into consideration oxygen

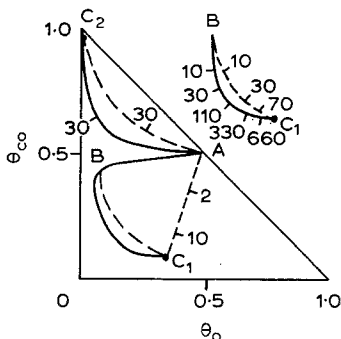


Fig. 26. Phase pattern of the system with kinetic functions (2)–(3) at $P_{O_2} = 6 \times 10^{-6}$ and $P_{CO} = 5 \times 10^{-6}$ Torr. C_1 = steady state at $T = 540$ K; C_2 = steady state at $T = 400$ K. Broken lines = trajectories at $D \approx 0$. The marks on the trajectories are the positions the system reaches at the times indicated.

diffusion into the catalyst bulk proves to be essential for the interpretation of slow relaxation processes.

The dynamics of critical phenomena in catalytic oxidation over platinum, in particular of CO oxidation, has been examined comprehensively [156–160]. The authors [156–160] obtained a variety of interesting data concerning the “ignition” of this reaction and its dependence on the catalyst state. These data were interpreted on the basis of the above branched-chain model. It will be of interest to analyze the same data using our model.

Let us consider the phenomenon called a “memory effect”. The experiment was carried out as follows. The temperature was elevated up to that for the “ignition”. At first the reaction rate increased slowly (an induction period) and then the “ignition” started. This “ignition” was interrupted by switching off the electric current feeding the transmitter-catalyst. On further heating the transmitter up to the “ignition” temperature, “ignition” takes place without an induction period 10 min after “freezing” in the case of CO oxidation [156–160] or even after some hours in the case of the oxidation of NH_3 [161–164]. It is this phenomenon that is the “memory effect” (Fig. 27).

It was also shown that the induction period η_1 monotonically increases by increasing the “freezing” time η_2 up to a certain critical value $\eta_{2,\text{crit}}$. Above this value no “ignition” is possible. If one fixes the “ignition” temperature, T_1 , and decreases the “freezing” temperature, T_2 , the qualitative character of $\eta_1 = f(\eta_2)$ curves will be preserved but the value of $\eta_{2,\text{crit}}$ will rise. But if T_2 is fixed and T_1 is increased, the character of $\eta_1 = f(\eta_2)$ curves will also be preserved but only up to a certain temperature. After exceeding this temperature the curves change qualitatively (Fig. 28).

In terms of the branched-chain model this fact can be interpreted as follows. On rapidly cooling the catalyst, we preserve the high concentration of active centres achieved during “ignition”. Hence, next time, “ignition” will take place without an induction period. However, we believe the “memory effect” can be interpreted on the basis of the ideal adsorbed layer model.

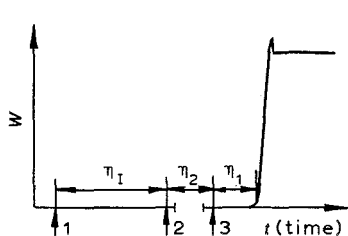


Fig. 27. Time dependence of the reaction rate during the “ignition” process. 1, Achievement of “ignition” temperature T_1 ; 2, “freezing” at T_2 ; 3, repeated achievement of T_1 .

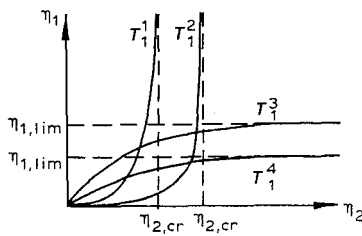


Fig. 28. Dependence of the induction period η_1 on the “erasure” time η_2 at fixed temperature T_2 : $T_1^1 < T_1^2 < T_1^3 < T_1^4$.

Let us carry out a numerical experiment. Assume that we have taken the initial state of the catalyst corresponding to the "upper" steady-state branch at $T_1 (T_- < T_1 < T_+)$. Then the system will be maintained at a temperature $T_2 (T_2 \ll T_-)$ during the time η_2 . The system will tend to its steady state corresponding to the "lower" branch. But its relaxation can be quite slow. When, after the time η_2 , the temperature is again increased to T_1 , the catalyst state can still remain in the attraction region of the "upper" branch. The critical time η_{2crit} is the time during which the system enters into the attraction region of the lower branch. The difference in the behaviour of η_{2crit} depends on the region chosen for the "freezing" temperature. "Far" from T_- , the lower T_2 , the lower the relaxation rate and the time η_{2crit} must increase. But there exists another possibility: "near" T_- , in the region of slow relaxations, the time for entering into the attraction region of the "lower" branch rises and, in principle, can be infinite.

Results of the numerical experiments are given in Fig. 29. We believe they represent all the peculiarities of the Barelko et al. dynamic experiment. The observed activation energy for the propagation of active centres found from the plotted dependence $\eta_1 = f(T)$ at a fixed $T_2 (T_1 > T_+, T_2 < T_-)$ [158] amounts to 100–150 kcal mol⁻¹ (Fig. 30). This value is close to that of the heat of sublimation for platinum. This correlation has been treated as an additional argument in favour of the branched-chain model. But our numerical experiment based on model (2)–(3) provides the same plotted dependence

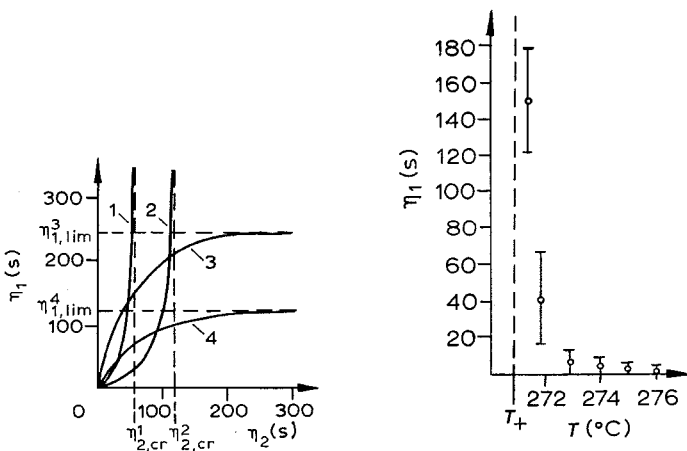


Fig. 29. Induction period η_1 as a function of the "erasure" time η_2 at various positions of T_1 with respect of $T_+ = 533$ K (calculated data). 1, $T_1 = 520$, $T_2 = 450$; 2, $T_1 = 520$, $T_2 = 400$; 3, $T_1 = 540$, $T_2 = 450$; 4, $T_1 = 550$, $T_2 = 450$ K.

Fig. 30. Induction period η_1 as a function of the "ignition" temperature T_1 at fixed T_2 (experimental data [158]).

and sufficiently high values for the observed activation energy (120 kcal mol⁻¹).

It can be attributed only to the fact that the system passes through the "bifurcation" point due to which relaxation processes are sharply retarded, and in the neighbourhood of this point steady state and relaxation characteristics are highly sensitive to the parameters.

Thus the Barelko et al. experimental data [156, 158] can be given a qualitative interpretation in terms of the non-linear kinetic models for the ideal adsorption layer.

4. "General" kinetic model and prediction of critical effects

One of the most essential problems in the construction of a "general" kinetic model is to describe both the high-vacuum and the normal pressure regions (we have discussed this problem more fully in Sect. 1).

Today a detailed model for the complex reaction of CO oxidation over metals can be constructed only in the high-vacuum region where there exist mechanisms obtained on the basis of the direct observation of the catalyst state and its surface composition. But of applied significance is also the region of pressures above 1 Torr for which such measurements are practically absent in the literature.

Nevertheless even now it is possible to apply the qualitative investigation of kinetic models corresponding to simple model mechanisms, not only for a description of the established experimental kinetic curves, but also for the prediction of kinetic regularities in the parametric region that has not been examined by experiment [165].

Let us illustrate this by the example of critical effects. For CO oxidation these effects were observed quite often at normal pressures but extremely rarely in the high-vacuum region (see Sect. 1). Meanwhile the above calculated data show that the critical effect can also be observed in this region. Steady-state diagrams (Figs. 2 and 3) demonstrate intervals for the conditions under which critical effects do exist. This contradiction has existed until recently.

Golchet and White [62] have shown the existence of hysteresis of kinetic origin for CO oxidation over Pt at low pressures ($\sim 10^{-7}$ Torr). The same is evidenced by other data [53, 77, 98, 150]. It is significant that the region for the effects given in Fig. 5(a) and found experimentally [62] is close to that calculated according to the model (2)-(3) with parameters from ref. 49 (Fig. 31).

A quantitative description for the kinetic dependences $W_{\text{CO}_2}(P_{\text{CO}})$ over Pt and Pd characterized by the presence of two stable steady-state branches for the reaction rate [62] was obtained [166] in terms of the adsorption mechanism [steps (1)-(3) of reaction (1)] taking into account semi-empirical dependences of the rate constants for CO adsorption and desorption on the surface

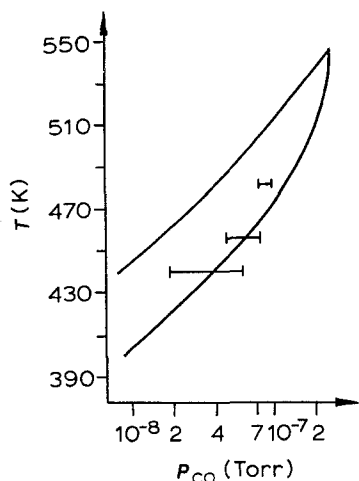
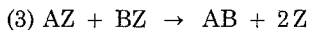
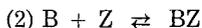
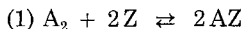


Fig. 31. Diagram for steady states of reaction (1) with parameters from ref. 49 ($P_{O_2} = 1 \times 10^{-7}$ Torr). The bars mark the width of the multiplicity region according to experimental data from ref. 62.

composition and temperature. Numerical modelling of experimental data [142] obtained under high vacuum shows the possibility of a fairly good quantitative description of critical effects in terms of system (2)–(3).

Let us now take normal conditions. For CO oxidation over Pt catalysts, sufficiently complete studies have been carried out to identify the dependence of the reaction rate on the CO concentration $W(C_{CO})$ and temperature $W(T)$. For these dependences we can observe specific critical effects. They are the clockwise hysteresis for $W(C_{CO})$ and counter-clockwise hysteresis for $W(T)$. It is these characteristics that we have obtained for the kinetic model of the adsorption mechanism.



But this mechanism is also valid for $W(C_{O_2})$ characterized by counter-clockwise hysteresis. Under normal pressures no such dependence has been found. There are only a few literature results evidencing the high parametric sensitivity of $W-C_{O_2}$ [53]. But these data have been obtained in the high vacuum region.

For our study we have chosen the CO oxidation reaction over a Pd catalyst with 0.5 wt.% Pd (2–3 mm grains) supported by non-porous porcelain. Experiments were carried out by Orlik et al. [167]. The CO and O_2 concentrations were ranged from 0.25 to 2 and from 1 to 8 vol.%, respective-

ly. The flow rate was 200 ml min^{-1} and $T = 420\text{--}700 \text{ K}$. It is in this system that a clockwise hysteresis for $W(C_{\text{CO}})$ and a counter-clockwise hysteresis for $W(T)$ were observed.

It has already been noted that counter-clockwise hysteresis can also exist in $W(C_{\text{O}_2})$. Just this peculiarity has been found experimentally in the above parametric range (Fig. 32).

The kinetic characteristics of the reaction exert a considerable effect on the CSTR behaviour. If the kinetic curve is of the type represented in Fig. 32, in some parametric range self-oscillations of the reaction rate are possible in CSTR. Figure 33 illustrates the case in which the curve for the reaction rate (1) and the straight line for the substance transfer into the

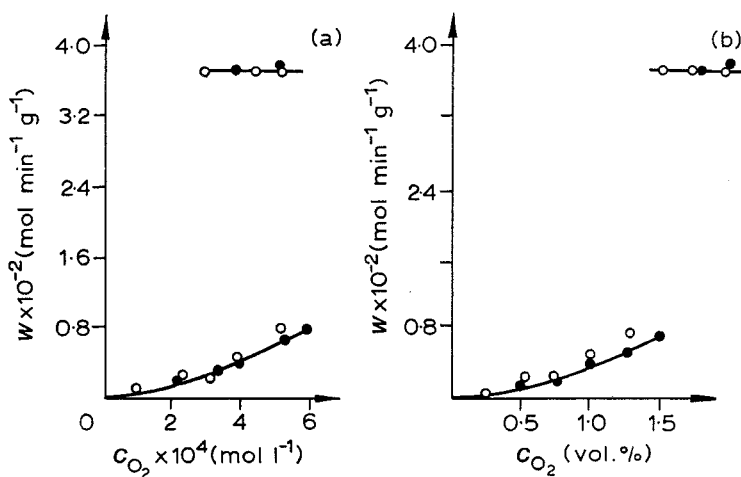


Fig. 32. Dependence of steady state reaction rate on O_2 concentration (a) and its initial concentration (b) at $T = 528 \text{ K}$.

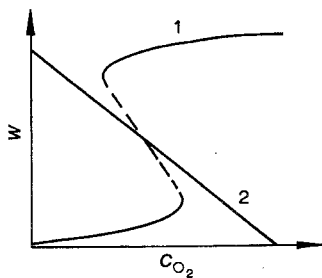


Fig. 33. Characteristics of isothermal CSTR: 1, kinetic reaction rate dependence; 2, straight line for substance transfer into environments.

environment (II) cross at a unique unstable point. As is known, it is in this case that self-oscillations can appear.

This situation was reproduced experimentally in the same system of CO oxidation over a Pd catalyst. The period of self-oscillations amounted to 20 min (at $T = 500$ K, $C_{CO} = 2.5\%$, and flow rate $V = 100$ ml min⁻¹) [168].

Thus it appears that the simple models for the ideal adsorbed layer can be used to predict the critical effects that have not previously been found experimentally. In particular, the results [146–148] permit us to interpret (and predict) the induction period for the reaction with long-term relaxation near critical transition (points of bifurcation) observed in the experimental studies of reactions characterized by critical effects [164, 169].

On the other hand, it is clear that the "ideal" models cannot describe the behaviour of complex catalytic reactions in complete detail. In particular, we cannot quantitatively explain the values of the self-oscillation periods obtained by Orlik et al. Secondly, for example, we have failed to describe the critical effects obtained by Barelko et al. in terms of model (2)–(3) corresponding to the two-route mechanism with the parameters taken from ref. 49 or ref. 142. Our calculated reaction rates proved to be at least two orders of magnitude higher than the experimental values. Apparently our models must be considerably modified, primarily in the region of normal pressures. It is necessary to take into account the formation of unreactive oxygen forms that considerably decrease the rate of CO₂ generation, the dependence of the reaction parameters on the surface composition and catalyst volume and finally the diffusion of oxygen into the catalyst.

There are also two factors that have already been noted in the numerical analysis of the kinetic model of CO oxidation: (1) fluctuations in the surface composition of the gas phase and temperature can lead to the fact that the "actual" multiplicity of steady states will degenerate into an unique steady state with high parametric sensitivity [170] and (2) due to the limitations on the observation time (which in real experiments always exists) we can observe a "false" hysteresis in the case when the steady state is unique. Apparently, "false" hysteresis will take place in the region in which the relaxation processes are slow.

Nevertheless, the above complicating factors are not reasons to refuse to investigate these simple models which permit us to predict the very fact of critical effects and their kinetic peculiarities.

References

- 1 I. Langmuir, *Trans. Faraday Soc.*, 17 (1922) 607.
- 2 I. Langmuir, *Trans. Faraday Soc.*, 17 (1922) 621.
- 3 O.V. Krylov, *Kinet. Katal.*, 21 (1980) 79.
- 4 R.L. Palmer and J.N. Smith, Jr., *J. Chem. Phys.*, 60 (1974) 1453.
- 5 V.F. Malakhov, V.A. Shmachkov and A.M. Kolchin, *Proc. All-Union Conf. on Heterogeneous Catalytic Reaction Mechanism*, Moscow, 1974, Prepr. NN 1-114, N 64.

- 6 T. Engel and G. Ertl, *Adv. Catal.*, 28 (1980) 1.
- 7 V.I. Savchenko, *Kinet. Katal.*, 21 (1980) 832.
- 8 C.T. Campbell and J.M. White, *J. Catal.*, 54 (1978) 289.
- 9 T. Matsushima and J.M. White, *J. Catal.*, 39 (1975) 265.
- 10 T. Matsushima, D.B. Almy, D.C. Foyt, J.S. Close and J.M. White, *J. Catal.*, 39 (1975) 277.
- 11 D.M. Collins, J.B. Lee and W.E. Spicer, *Surf. Sci.*, 55 (1976) 389.
- 12 P.R. Norton, *Surf. Sci.*, 47 (1975) 98.
- 13 D.M. Collins and W.E. Spicer, *Surf. Sci.*, 69 (1977) 85.
- 14 B.E. Nieuwenhuys and G.A. Somorjai, *Surf. Sci.*, 72 (1978) 8.
- 15 R.L. Palmer and J.N. Smith, Jr., *Catal. Rev. Sci. Eng.*, 12 (1975) 279
- 16 J.L. Gland and V.N. Korchak, *Surf. Sci.*, 75 (1978) 733.
- 17 W.H. Weinberg, C.M. Comrie and R.M. Lambert, *J. Catal.*, 41 (1976) 489.
- 18 H. Conrad, G. Ertl, J. Koch and E.E. Latta, *Surf. Sci.*, 43 (1974) 462.
- 19 D.I. Hagen, B.E. Nieuwenhuys, G. Rovida and G.A. Somorjai, *Surf. Sci.*, 57 (1976) 632.
- 20 I. Toyoshima and G.A. Somorjai, *Catal. Rev. Sci. Eng.*, 19 (1979) 105.
- 21 A.M. Bredshaw, *Surf. Sci.*, 80 (1979) 215.
- 22 R.W. McCabe and L.D. Schmidt, *Surf. Sci.*, 66 (1977) 101.
- 23 W.L. Winterbottom, *Surf. Sci.*, 36 (1973) 195.
- 24 R.R. Ford, *Adv. Catal.*, 21 (1970) 51.
- 25 A.V. Sklyarov, *Probl. Kinet. Katal.*, 16 (1975) 238.
- 26 R.J. Madix and J. Benziger, *Annu. Rev. Phys. Chem.*, 29 (1978) 285.
- 27 C.O. Bennett, *Catal. Rev. Sci. Eng.*, 13 (1976) 121.
- 28 B. Weber and A. Cassuto, *Kinet. Katal.*, 24 (1983) 796.
- 29 G.K. Boreskov and V.I. Savchenko, *Commun. Dep. Chem. Bulg. Acad. Sci.*, 16 (1983) 57.
- 30 V.P. Ivanov, G.K. Boreskov, V.I. Savchenko and V.L. Tataurov, *Kinet. Katal.*, 24 (1983) 931.
- 31 V.I. Savchenko, G.K. Boreskov, A.V. Kalinkin and A.N. Salanov, *Kinet. Katal.*, 24 (1983) 1154.
- 32 G. Ertl, *CRC Crit. Rev. Solid State Mater. Sci.*, 10 (1982) 349.
- 33 G. Ertl, *Catal. Sci. Technol.*, 4 (1984) 209.
- 34 G. Ertl, *Surf. Sci.*, 152/153 (1985) 328.
- 35 B.E. Nieuwenhuys, *Surf. Sci.*, 126 (1983) 307.
- 36 G. Ertl and R. Rau, *Surf. Sci.*, 15 (1969) 443.
- 37 A.V. Sklyarov, I.I. Tretyakov, B.R. Shub and S.Z. Roginskii, *Dokl. Akad. Nauk SSSR*, 189 (1969) 1302.
- 38 I.I. Tretyakov, A.V. Sklyarov and B.R. Shub, *Kinet. Katal.*, 11 (1970) 166.
- 39 I.I. Tretyakov, A.V. Sklyarov and B.R. Shub, *Kinet. Katal.*, 12 (1971) 996.
- 40 H.P. Bonzel and R. Ku, *J. Vac. Sci. Technol.*, 9 (1972) 663.
- 41 K. Christman and G. Ertl, *Z. Naturforsch.*, 28 (1973) 1144.
- 42 Y. Nishiyama and H. Wise, *J. Catal.*, 32 (1974) 50.
- 43 H.P. Bonzel and R. Ku, *Surf. Sci.*, 33 (1972) 91.
- 44 G. Ertl, and J. Koch, *Proc. 5th Int. Congr. Catal., North-Holland, Amsterdam, 1972*, pp. 969-977.
- 45 W.L. Winterbottom, *Surf. Sci.*, 36 (1973) 205.
- 46 V.L. Kuchaev and L.M. Nikitushina, *Proc. All-Union Conf. on Heterogeneous Catalytic Reaction Mechanism, Moscow, 1974, Prepr. N 1-114, N 59*.
- 47 T.E. Madey, H.A. Engelhard and D. Menzel, *Surf. Sci.*, 48 (1975) 304.
- 48 N. Pasia, A. Cassuto, A. Pentenero and B. Weber, *J. Catal.*, 41 (1976) 455.
- 49 A. Cassuto, Yu. I. Kuznetsov, C. Miniscloux N. Pasia, A. Pentenero, H. Van Landegem and B. Weber, *II Colloque Franco-Sovietique: Simulation et Modelisation de Processus et de Reacteurs Catalytiques, Novosibirsk, 1975, Institute of Catalysis, Novosibirsk, 1976*, pp. 12-30.
- 50 J. Küppers and A. Plagge, *J. Vac. Sci. Technol.*, 13 (1976) 259.
- 51 J.A. Strozier, Jr., *Surf. Sci.*, 87 (1979) 161.

- 52 T. Engel and G. Ertl, *J. Chem. Phys.*, 69 (1978) 1267.
53 T. Matsushima, *Bull. Chem. Soc. Jpn.*, 51 (1978) 1956.
54 T. Matsushima, M. Hashimoto and I. Toyoshima, *J. Catal.*, 58 (1979) 303.
55 J.L. Taylor, D.E. Ibbotson and W.H. Weinberg, *Surf. Sci.*, 90 (1979) 37.
56 C.T. Campbell, S.-K. Shi and J.M. White, *J. Phys. Chem.*, 83 (1979) 2255.
57 J. Küppers and A. Plagge, *Z. Naturforsch. Teil A.*, 34 (1979) 81.
58 P.A. Zhdan, G.K. Boreskov, W.F. Egelhoff, Jr. and W.H. Weinberg, *Surf. Sci.*, 61 (1976) 377.
59 V.P. Ivanov, G.K. Boreskov, V.I. Savchenko, W.F. Egelhoff, Jr. and W.H. Weinberg, *J. Catal.*, 48 (1977) 269.
60 T. Matsushima and J.M. White, *Surf. Sci.*, 67 (1977) 122.
61 T. Matsushima, D.B. Almy and J.M. White, *Surf. Sci.*, 67 (1977) 89.
62 A. Golchet and J.M. White, *J. Catal.*, 53 (1978) 251.
63 M. Wilf and P.T. Dawson, *Surf. Sci.*, 65 (1977) 399.
64 M. Procop and J. Völter, *Z. Phys. Chem. (Leipzig)*, 250 (1972) 387.
65 B. Weber, J. Fusy and A. Cassuto, *J. Chim. Phys.*, 66 (1974) 708.
66 G. Kneringer and F.P. Netzer, *Surf. Sci.*, 49 (1975) 125.
67 V.P. Ivanov, V.I. Savchenko, G.K. Boreskov and K.S. Taylor, *Kinet. Katal.*, 19 (1978) 210.
68 M. Alnot, J. Fusy and A. Cassuto, *Surf. Sci.*, 71 (1978) 467.
69 H.P. Bonzel and R. Ku, *Surf. Sci.*, 40 (1973) 85.
70 P.A. Zhdan, G.K. Boreskov, A.I. Boronin, W.H. Egelhoff, Jr. and W.H. Weinberg, *Surf. Sci.*, 61 (1976) 25.
71 P.D. Reed, C.M. Comrie and R.M. Lambert, *Surf. Sci.*, 64 (1977) 603.
72 V.D. Belov, Yu.K. Ustinov and A.P. Komar, *Kinet. Katal.*, 18 (1977) 1448.
73 G.M. Bliznyakov, and M.P. Kiskinova, *J. Catal.*, 61 (1980) 299.
74 R. Ducros and R.P. Merrill, *Surf. Sci.*, 55 (1976) 227.
75 V.L. Kuchaev and L.M. Nikitushina, *Zh. Fiz. Khim.*, 54 (1980) 1256.
76 J.L. Taylor, D.E. Ibbotson and W.H. Weinberg, *Surf. Sci.*, 79 (1979) 349.
77 V.L. Tataurov and V.I. Ivanov, *Instationary Processes in Catalysis*, Institute of Catalysis, Novosibirsk, 1979, Part 2, pp. 170-175 (in Russian).
78 V.P. Ivanov, Ph.D. Dissertation, Institute of Catalysis, Novosibirsk, 1978 (in Russian).
79 D.J. Castner and G.A. Somorjai, *Chem. Rev.*, 79 (1979) 233.
80 G. Doyen and G. Ertl, *J. Chem. Phys.*, 62 (1975) 2957.
81 L.D. Roefols, R.L. Park and T.L. Einstein, *J. Vac. Sci. Technol.*, 16 (1979) 487.
82 M. Bowker and D.A. King, *Surf. Sci.*, 71 (1978) 583.
83 C.T. Campbell, D.C. Foyt and J.M. White, *J. Phys. Chem.*, 81 (1977) 491.
84 R.W. McCabe and L.D. Schmidt, *Surf. Sci.*, 60 (1976) 85.
85 V.V. Gorodetskii and V.I. Savchenko, *Proc. 5th Int. Congr. Catal.*, North-Holland, Amsterdam, 1972, p. 527.
86 H. Niehus and G. Gomsa, *Surf. Sci.*, 93 (1980) L147.
87 P.A. Zhdan, A.P. Shepelin, A.I. Boronin, G.K. Boreskov, W.H. Weinberg and W.F. Egelhoff, Jr., *J. Catal.*, 62 (1980) 180.
88 M.D. Smolikov, and V.I. Savchenko, *React. Kinet. Catal. Lett.*, 12 (1979) 457.
89 M.J. Mummey and L.D. Schmidt, *Surf. Sci.*, 91 (1980) 301.
90 A.N. Salanov and V.I. Savchenko, *React. Kinet. Catal. Lett.*, 29 (1985) 101.
91 M. Salmeron, L. Brewer and G.A. Somorjai, *Surf. Sci.*, 112 (1981) 207.
92 V.I. Savchenko, V.P. Ivanov and K.A. Dadayan, *Proc. 5th Soviet-Japan Seminar Catal.*, FAN Tashkent, 1979, p. 244 (in Russian).
93 C.M. Comrie and W.H. Weinberg, *J. Chem. Phys.*, 64 (1976) 250.
94 J.L. Taylor, D.E. Ibbotson and W.H. Weinberg, *Surf. Sci.*, 78 (1978) 259.
95 G. Ertl, M. Neumann and K.M. Streit, *Surf. Sci.*, 64 (1977) 393.
96 J.C. Tracy and D.M. Palmberg, *J. Chem. Phys.*, 51 (1969) 4852.
97 R. Ku, N.A. Gjostein and H.P. Bonzel, *Surf. Sci.*, 64 (1977) 465.
98 T. Engel and G. Ertl, *Advan. Catal.*, 28 (1980) 1.

- 99 P.A. Zhdan, G.K. Borekov, A.I. Boronin, A.P. Shepelin, S.P. Withrow and W.H. Weinberg, *Appl. Surf. Sci.*, 3 (1979) 145.
- 100 P.A. Zhdan, G.K. Borekov, A.I. Boronin, W.F. Egelhoff and W.H. Weinberg, *Chem. Phys. Lett.*, 44 (1976) 528.
- 101 P.A. Zhdan, G.K. Borekov, A.I. Boronin, A.P. Shepelin, W.F. Egelhoff and W.H. Weinberg, *Surf. Sci.*, 71 (1978) 267.
- 102 V.A. Shmachkov, V.F. Malakhov, V. Yu. Vasilyev and A.M. Kolchin, *Kinet. Katal.*, 18 (1977) 572.
- 103 V.F. Malakhov, V.A. Shmachkov and A.M. Kolchin, II Colloque Franco-Sovietique Seminar: Simulation et Modelisation de Processus et de Reacteurs Catalytiques, Novosibirsk, 1975, Institute of Catalysis, Novosibirsk, 1976, p. 49.
- 104 V.A. Shmachkov, V.F. Malakhov and A.M. Kolchin, *Probl. Kinet. Katal.*, 17 (1978) 170.
- 105 V.F. Malakhov, V.A. Shmachkov, V. Yu. Vasilyev and A.M. Kolchin, *Instationary Processes in Catalysis*, Institute of Catalysis, Novosibirsk, 1979, Part 1, pp. 76-82.
- 106 V.P. Ivanov, G.K. Borekov, V.I. Savchenko, V.L. Tataurov, W.H. Weinberg and W.F. Egelhoff, Jr., *Dokl. Akad. Nauk SSSR*, 249 (1979) 642.
- 107 N. Pasia, B. Weber and A. Pentenero, *Surf. Sci.*, 49 (1975) 330.
- 108 M. Alnot, J. Fusy and A. Cassuto, *Surf. Sci.*, 57 (1976) 651.
- 109 H. Hopster, H. Ibach and G. Gomsa, *J. Catal.*, 46 (1977) 37.
- 110 J.M. White and A. Golchet, *J. Chem. Phys.*, 66 (1977) 5744.
- 111 M. Ali and P. Hugo, *Kinetics of Physicochemical Oscillations. Discussion Meeting, Aachen, 1979, Prepr.*, Vol. 1, p. 161.
- 112 H.P. Bonzel and J.J. Burton, *Surf. Sci.*, 52 (1975) 223.
- 113 H. Heyne and F.C. Tompkins, *Proc. R. Soc. London Ser. A*, 292 (1966) 460.
- 114 J.A. Strozier, Jr., J.G. Gosgrove and D.A. Fisher, *Surf. Sci.*, 82 (1979) 481.
- 115 G.M. Schwab and K. Gossner, *Z. Phys. Chem. NF*, 161 (1958) 39.
- 116 R.F. Baddour, M. Modell and U.K. Heusser, *J. Phys. Chem.*, 72 (1968) 3621.
- 117 S.E. Voltz, C.R. Morgan, D. Liederman and S.M. Jakob, *Ind. Eng. Chem. Prod. Res. Dev.*, 12 (1973) 294.
- 118 S.J. Stephens, *J. Phys. Chem.*, 63 (1959) 188.
- 119 G.K. Hori and L.D. Schmidt, *J. Catal.*, 38 (1975) 335.
- 120 G. Eigenberger, 4th Int./6th Eur. Symp. Chem. React. Eng., Heidelberg, Dechema, 1976, Vol. 1, *Contr. Papers (Prepr.)*, Frankfurt am Main, 1976, pp. 290-299.
- 121 G. Eigenberger, *Chem. Eng. Sci.*, 33 (1978) 1255, 1263.
- 122 R.K. Herz and S.P. Marin, *J. Catal.*, 65 (1980) 281.
- 123 E. McCarthy, J. Zahradnik, G.C. Kuczynskii and J.J. Carberry, *J. Catal.*, 39 (1975) 29.
- 124 C. Miniscloux, H. Van Landegem, Yu. Kuznetsov, A. Cassuto, N. Pasia, A. Pentenero and B. Weber, II Colloque Franco-Sovietique: Simulation et Modelisation de Processes et de Reactours Catalytiques, Novosibirsk, 1975, Institute of Catalysis, Novosibirsk, 1976, pp. 69-98.
- 125 N.W. Cant, P.C. Hicks and B.S. Lennon, *J. Catal.*, 54 (1978) 372.
- 126 H.P. Bonzel, *Surf. Sci.*, 68 (1977) 236.
- 127 M. Boudart, D.M. Collins, F.V. Hanson and W.E. Spicer, *J. Vac. Sci. Technol.*, 14 (1977) 441.
- 128 M. Boudart and F.V. Hanson, *J. Catal.*, 53 (1978) 56.
- 129 R. Dagonnier and J. Nuyts, *J. Chem. Phys.*, 65 (1976) 2061.
- 130 B.S. Sales, J.E. Turner and M.B. Maple, *Surf. Sci.*, 114 (1982) 381.
- 131 B.K. Cho, *Ind. Eng. Chem. Fundam.* 22 (1983) 410.
- 132 D.W. Goodman, *Annu. Rev. Phys. Chem.*, 37 (1986) 425.
- 133 S.H. Oh, G.B. Fisher, J.E. Carpenter and D.W. Goodman, *J. Catal.*, 100 (1986) 360.
- 134 D.J. Kaul, R. Sant and E.E. Wolf, *Chem. Eng. Sci.*, 42 (1987) 1399.
- 135 M.Z. Lazman, G.S. Yablonskii and V.I. Marshneva, *Thermodynamics of Irreversible Processes*, Nauka, Moscow, 1987, pp. 246-253 (in Russian).

- 136 G.S. Yablonskii, V.I. Bykov, M.G. Slin'ko and Yu.I. Kuznetsov, Dokl. Akad. Nauk SSSR, 229 (1976) 917.
- 137 D.A. Frank-Kamenetskii, Diffusion and Heat Transfer in Chemical Kinetics, Nauka, Moscow, 1987, 3rd edn. (in Russian); Plenum Press, New York, 1969.
- 138 V.I. Bykov, G.S. Yablonskii and V.I. Elokhin, Kinet. Katal., 20 (1979) 1029.
- 139 V.I. Bykov, G.S. Yablonskii and M.G. Slin'ko, Dokl. Akad. Nauk SSSR, 229 (1976) 1356.
- 140 V.I. Elokhin, V.I. Bykov, M.G. Slin'ko and G.S. Yablonskii, Dokl. Akad. Nauk SSSR, 238 (1978) 615.
- 141 V.I. Bykov, Yu.G. Zarkhin and G.S. Yablonskii, Teor. Eksp. Khim., 16 (1980) 487.
- 142 V.P. Ivanov, V.I. Elokhin, G.S. Yablonskii, V.I. Savchenko and V.L. Tataurov, Kinet. Katal., 22 (1981) 1040.
- 143 V.P. Ivanov, V.I. Savchenko, and V.L. Tataurov, Zh. Tekh. Fiz., 51 (1981) 392.
- 144 V.P. Ivanov, G.K. Boreskov, V.I. Savchenko and V.L. Tataurov, Kinet. Katal., 24 (1983) 931.
- 145 V.P. Zhdanov and K.I. Zamaraev, Catal. Rev. Sci. Eng., 24 (1982) 373.
- 146 A.N. Gorban', V.I. Elokhin, V.M. Cheresiz and G.S. Yablonskii, Instationary Processes in Catalysis, Institute of Catalysis, Novosibirsk, 1979, Part 1, pp. 83-88 (in Russian).
- 147 A.N. Gorban', V.M. Cheresiz, V.I. Elokhin and G.S. Yablonskii, Mathematical Methods in Chemistry, Vol. 2, Qualitative Methods, CNIITENeftekhim, Moscow, 1980, pp. 53-60 (in Russian).
- 148 A.N. Gorban' and V.M. Cheresiz, Dokl. Akad. Nauk SSSR, 261 (1981) 1050; Sov. Math. Dokl., 24 (1981) 645.
- 149 V.I. Bykov, A.N. Gorban' and T.P. Pushkareva, Teor. Eksp. Khim., 12 (1982) 776.
- 150 J.L. Taylor, D.E. Ibbotson and W.H. Weinberg, J. Catal., 62 (1980) 1.
- 151 D.E. Beck and E. Miyazaki, Surf. Sci., 39 (1973) 37; 48 (1975) 473.
- 152 H.-C. Chang and W.H. Weinberg, Surf. Sci., 65 (1977) 153.
- 153 A.G. Merzhanov and V.N. Bloshenko, Dokl. Akad. Nauk SSSR, 242 (1978) 1118.
- 154 B.S. Balzhinimaev, M.A. Shmeleva, V.I. Timoshenko and G.R. Kotelnikov, Proc. 2nd All-Union Conf. on Kinet. of Catal. Reactions (Kinetics-2), Vol. 3, Institute of Catalysis, Novosibirsk, 1975, pp. 85-91 (in Russian).
- 155 O.A. Makhotkin, V.I. Elokhin and G.S. Yablonskii, Mathematical Methods in Chemistry, Vol. 1, Numerical Methods, CNIITENeftekhim, Moscow, 1980, pp. 77-85 (in Russian).
- 156 V.V. Barelko and A.G. Merzhanov, Probl. Kinet. Katal., 17 (1978) 182.
- 157 S.A. Zhukov and V.V. Barelko, Dokl. Akad. Nauk SSSR, 229 (1976) 655.
- 158 V.V. Barelko and S.A. Zhukov, To the Stability of the CO Oxidation Processes on Platinum in the Lumped- and Distributed-Parameter Systems. Preprint Otd. Instit. Khim. Fiz., Chernogolovka, 1979 (in Russian).
- 159 S.A. Zhukov, Ph.D. Dissertation, Otd. Inst. Khim. Fiz., Chernogolovka, 1980 (in Russian).
- 160 V.V. Barelko and Yu.E. Volodin, Dokl. Akad. Nauk SSSR, 216 (1976) 1080.
- 161 Yu.E. Volodin, V.V. Barelko and P.I. Khal'zov, Chem. Eng. Commun., 18 (1982) 271.
- 162 V.V. Barelko, Kinet. Katal., 14 (1973) 196.
- 163 V.V. Barelko and Yu.E. Volodin, Dokl. Akad. Nauk SSSR, 211 (1973) 1373.
- 164 V.V. Barelko and Yu.E. Volodin, Kinet. Katal., 17 (1976) 683.
- 165 V.I. Elokhin and G.S. Yablonskii, Proc. 5th Int. Symp. on Heterog. Catal., Varna, 1983, Part II, pp. 169-174.
- 166 J.R. Creighton, F.-H. Tseng, J.M. White and J.S. Turner, J. Phys. Chem., 85 (1981) 703.
- 167 S.N. Orlik, V.G. Vysochenko, M.G. Martsenyuk-Kukharuk, A.V. Fesenko, G.S. Yablonskii and G.P. Korneichuk, Dokl. Akad. Nauk SSSR, 253 (1980) 915.
- 168 S.N. Orlik, G.S. Yablonskii and G.P. Korneichuk, React. Kinet. Catal. Lett., 18 (1981) 329.
- 169 R.E. Lagos, B.S. Sales and H. Suhl, Surf. Sci., 82 (1979) 525.
- 170 A.V. Grechannikov and G.S. Yablonskii, React. Kinet. Catal. Lett., 19 (1982) 321.